Received: 19 June 2024 | Revised: 25 August 2024 | Accepted: 29 August 2024

DOI: 10.1002/ardp.202400504

ARCH PHARM DPhG
Archiv der Pharmazie

FULL PAPER

# Novel benzothiazole/benzothiazole thiazolidine-2,4-dione derivatives as potential FOXM1 inhibitors: In silico, synthesis, and in vitro studies

Khaled A. N. Abusharkh[1,2,3] | Ferah Comert Onder[4] | Venhar Çınar[5] | Alper Onder[2] | Merve Sıkık[6] | Zuhal Hamurcu[5] | Bulent Ozpolat[7] | Mehmet Ay[2]

[1]Department of Chemistry, School of Graduate Studies, Çanakkale Onsekiz Mart University, Çanakkale, Türkiye

[2]Department of Chemistry, Natural Products and Drug Research Laboratory, Faculty of Science, Çanakkale Onsekiz Mart University, Çanakkale, Türkiye

[3]Department of Chemistry and Chemical Technology, Faculty of Science and Technology, Al-Quds University, East Jerusalem, Palestine

[4]Department of Medical Biology, Faculty of Medicine, Çanakkale Onsekiz Mart University, Çanakkale, Türkiye

[5]Department of Medical Biology, Faculty of Medicine, Erciyes University, Kayseri, Türkiye

[6]Department of Medical System Biology, School of Graduate Studies, Çanakkale Onsekiz Mart University, Çanakkale, Türkiye

[7]Department of Nanomedicine, Houston Methodist Neal Cancer Center, Houston Methodist Research Institute, Houston, Texas, USA

**Correspondence**
Ferah Comert Onder, Department of Medical Biology, Faculty of Medicine, Çanakkale Onsekiz Mart University, 17020 Çanakkale, Türkiye.
Email: ferahcomertonder@comu.edu.tr

Bulent Ozpolat, Department of Nanomedicine, Houston Methodist Neal Cancer Center, Houston Methodist Research Institute, Houston, TX 77030-2707, USA.
Email: bozpolat@houstonmethodist.org

Mehmet Ay, Department of Chemistry, Natural Products and Drug Research Laboratory, Faculty of Science, Çanakkale Onsekiz Mart University, 17020 Çanakkale, Türkiye.
Email: mehmetay06@comu.edu.tr

**Funding information**
Al-Quds University; Council of Higher Education of Türkiye (YÖK Palestine Scholarship); Çanakkale Onsekiz Mart University Research Coordination Unit, Grant/Award Number: FDK-2022-4145

## Abstract

The oncogenic transcription factor FOXM1 overexpressed in breast and other solid cancers, is a key driver of tumor growth and progression through complex interactions, making it an attractive molecular target for the development of targeted therapies. Despite the availability of small-molecule inhibitors, their limited specificity, potency, and efficacy hinder clinical translation. To identify effective FOXM1 inhibitors, we synthesized novel benzothiazole derivatives (**KC10–KC13**) and benzothiazole hybrids with thiazolidine-2,4-dione (**KC21–KC36**). These compounds were evaluated for FOXM1 inhibition. Molecular docking and molecular dynamics simulation analysis revealed their binding patterns and affinities for the FOXM1-DNA binding domain. The interactions with key amino acids such as Asn283, His287, and Arg286, crucial for FOXM1 inhibition, have been determined with the synthesized compounds. Additionally, the molecular modeling study indicated that **KC12**, **KC21**, and **KC30** aligned structurally and interacted similarly to the reference compound FDI-6. In vitro studies with the MDA-MB-231 breast cancer cell line demonstrated that **KC12**, **KC21**, and **KC30** significantly inhibited FOXM1, showing greater potency than FDI-6, with $IC_{50}$ values of 6.13, 10.77, and 12.86 µM, respectively, versus 20.79 µM for FDI-6. Our findings suggest that **KC12**, **KC21**, and **KC30** exhibit strong activity as FOXM1 inhibitors and may be suitable for in vivo animal studies.

KEYWORDS
Benzothiazole, FOXM1 inhibitors, In vitro, MD simulation, TNBC

## 1 | INTRODUCTION

The Forkhead box M1 (FOXM1) transcription factor has emerged as a key regulator of various cellular processes essential for cancer progression, including cell proliferation, metastasis, angiogenesis, and drug resistance.[1–4] Aberrant expression of FOXM1 is frequently observed in a wide range of human cancers, including triple-negative breast cancer (TNBC),[5,6] and is associated with poor prognosis and aggressive tumor behavior.[7,8] Given its critical role in tumorigenesis and cancer progression, FOXM1 has garnered significant interest as a promising therapeutic target for solid cancers.[2]

Breast cancer stands as the most prevalent malignancy among women and ranks as the second leading cause of cancer-related mortality. TNBC, a distinct subtype, exhibits aggressive behavior, heightened recurrence rates, and poor prognosis compared to other breast cancer subtypes.[9–12] Given the limited treatment options and the absence of effective targeted therapies, there exists an urgent imperative to identify novel therapeutic targets and devise highly efficacious treatment modalities for TNBC patients.[3,11] Notably, overexpression of FOXM1 has been documented in TNBC, correlating with tumor aggressiveness, metastatic potential, and diminished overall survival rates.[12,13] FOXM1 promotes breast cancer cell proliferation, invasion, and metastasis through its transcriptional activation of genes involved in the cell cycle, angiogenesis, and epithelial–mesenchymal transition (EMT).[14,15] In previous studies,[4,12,16–20] we validated FOXM1 as a promising molecular target for TNBC and demonstrated that in vivo genetic targeting of FOXM1 using siRNA suppresses TNBC tumor growth in mouse models. Additionally, we elucidated the regulatory role of FOXM1 in modulating the expression of eukaryotic elongation factor 2 kinase (eEF2K), thereby promoting proliferation, invasion, and tumorigenesis in human TNBC cells. Furthermore, our investigations revealed the involvement of FOXM1 in autophagy regulation by transcriptionally controlling the expression of Beclin-1 and LC3 genes in human triple-negative breast cancer cells. On the other hand, FOXM1 regulates the expression of key genes like Cyclin D1, MMP-2, and VEGF, contributing to breast cancer progression.[14,15] In vitro gene knockdown studies in other cancers have underscored the significance of inhibiting FOXM1's transcriptional activity, leading to reduced cell proliferation migration and invasion across diverse cancer cell types, including TNBC,[4,10,12,20,21] but also in the prostate,[22] brain,[23] ovary,[7,24] lung,[25] colon,[26,27] and liver cancers.[28,29]

Overall, in vitro and in vivo findings collectively emphasize the multifaceted role of FOXM1 in the pathobiology of TNBC and other solid cancers, its critical role in promoting aggressive phenotype, and its potential as an ideal therapeutic target. Although various inhibitors have been identified to target FOXM1, none of these compounds were translated to clinical trials, and currently, there are no FDA approved inhibitors for targeting FOXM1.

Heterocycles, particularly benzothiazole, serve as crucial pharmacophores, offering diverse pharmacological activities and forming privileged chemical structures.[30] Benzothiazole, found in both terrestrial and marine compounds, is integral to numerous natural products with medicinal and pharmaceutical applications.[31] With a wide spectrum of biological activities, benzothiazole derivatives demonstrate anti-inflammatory,[32] antidiabetic,[33] antimicrobial,[34] and antitumor properties.[35] These compounds exhibit significant efficacy against various cancers,[35] including colon, liver, ovarian, non-small cell lung, and breast cancers.[36–39] Benzothiazole derivatives hold great promise as potential candidates for the development of novel therapeutics, particularly for targeting cancer[39] (Figure 1). On the other hand, thiazolidine-2,4-dione (THZ) is an important structural motif in medicinal organic chemistry, with broad biological activities including antibacterial,[40] antimicrobial,[41] anti-inflammatory,[42] and anticancer effects.[41,43] Both THZ and thiazole derivatives are key frameworks in drug design, displaying diverse pharmacological effects, particularly anticancer properties.[44,45] Several drug candidates with the THZ moiety (Figure 1) suppress cell proliferation in breast cancer cells, while thiazole derivatives show potential as anticancer agents.[45,46] These findings underscore THZ's significance in drug discovery for combating cancer and other diseases. Therefore, in the current study, we focused on benzothiazole and benzothiazole thiazolidine-based compounds to identify potential FOXM1 inhibitors.

In this study, we present the in silico studies, including molecular docking, dynamics, ADME, and synthesis of novel benzothiazole/benzothiazole-thiazolidine-2,4-dione derivatives, along with the evaluation of their anticancer activity in in vitro TNBC models as potential FOXM1 inhibitors.

## 2 | RESULTS AND DISCUSSION

### 2.1 | Chemistry

The outlined synthetic approach for the synthesis of the designated compounds (**KC10–KC13** and **KC21–KC36**) is described in Schemes 1 and 2.

Compounds **KC10–KC13** were synthesized through a three-step process (Scheme 1). The synthesis began with the cyclocondensation of 2-aminobenzenethiol with 4-hydroxy-3-methoxybenzaldehyde to yield 4-(benzo[d]thiazol-2-yl)-2-methoxyphenol (**3**). Subsequently, the reaction of substituted aniline/amine with bromoacetyl bromide in the presence of $K_2CO_3$ provided the corresponding (**KC10–KC13 (b)**) derivatives. Finally, compounds **KC10-KC13** were obtained by the reaction of 4-(benzo[d]thiazol-2-yl)-2-methoxyphenol (**3**) and various (**KC10–KC13 (b)**) derivatives under nitrogen in anhydrous *N*,*N*-dimethylformamide containing powdered anhydrous $K_2CO_3$, resulting in the formation of the corresponding 2-(4-(benzo[d]thiazol-2-yl)-2-methoxyphenoxy)-*N*-(substituted benzyl/phenyl) acetamide (**KC10–KC13**) with the yields ranging from 5% to 72%.

The general procedure for the synthesis of the designated compounds (**KC21–KC36**) was achieved through the versatile and efficient synthetic route outlined in Scheme 2. The starting material, thiazolidine-2,4-dione (THZ), was prepared by the condensation of thiourea with bromoacetic acid in the presence of hydrobromic acid. Subsequently, THZ underwent further condensation via the Knoevenagel condensation reaction with the appropriate aromatic

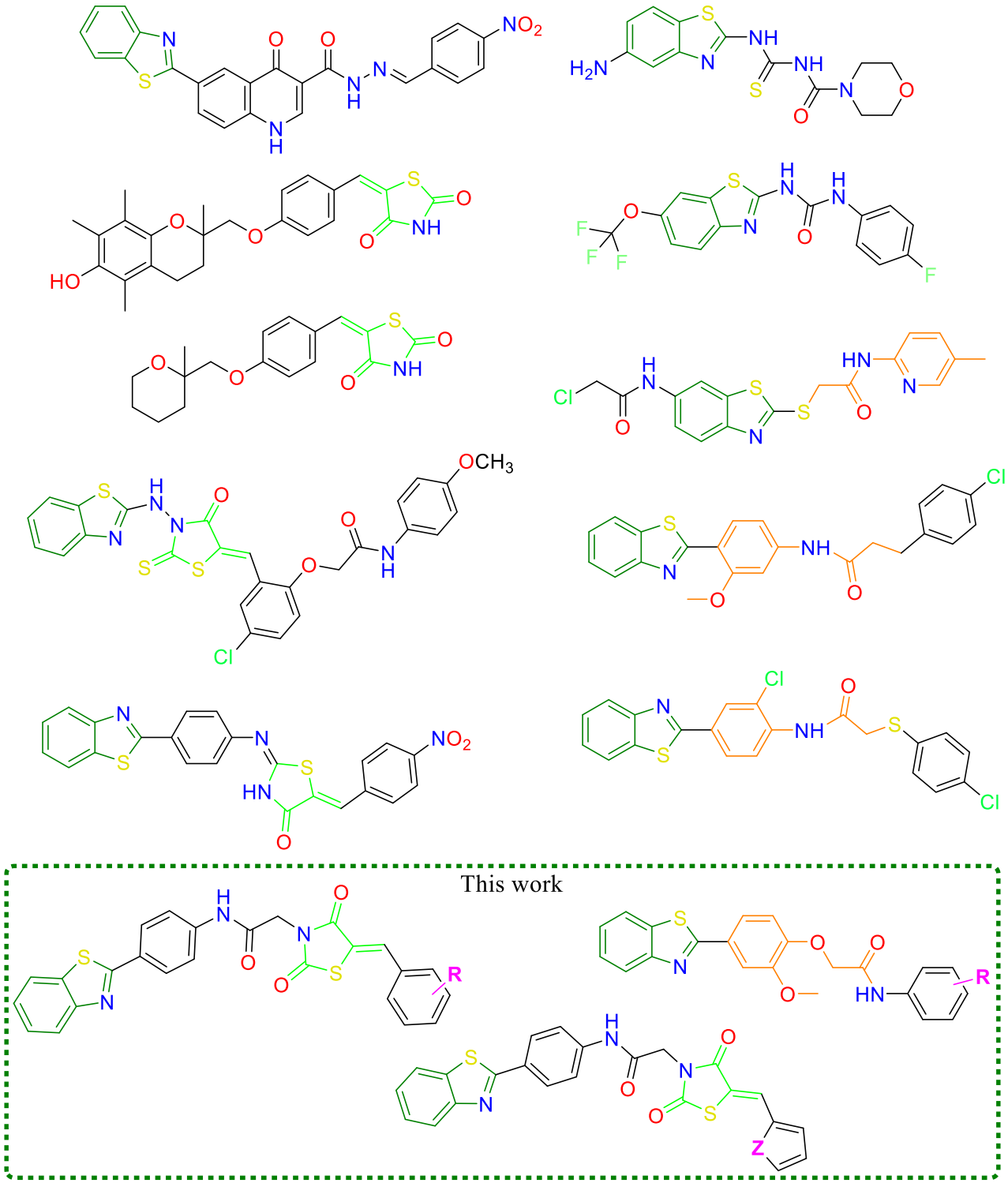


**FIGURE 1** Anticancer agents containing benzothiazole and thiazolidine-2,4-dione scaffolds along with the structure of synthesized compounds in this study.

aldehyde to yield the corresponding Knoevenagel compounds (**KC21–KC36 (d)**). The synthesis of these Knoevenagel compounds (**KC21–KC36 (d)**) involved two different condensation methods (vi and vii).[47,48] Method (iv) involved refluxing the reactants in sodium acetate (7.5 mol%) and glacial acetic acid as the solvent. Furthermore, the method (iv) involved condensing the reactants at 110°C in an oil bath under solvent-free reaction conditions using 10 mol% TBAB as a catalyst. The utilization of both methods a and b was required by the encountered limitations in exclusively employing method b for the synthesis of all compounds.

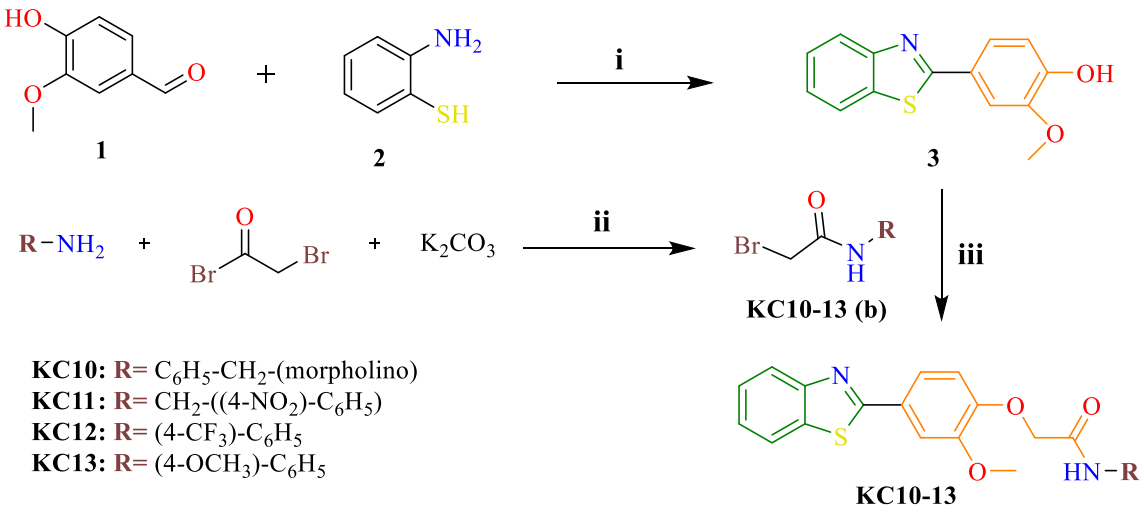


**SCHEME 1** Preparation of benzothiazole derivative **KC10–KC13**. (i) $NH_4Cl$, DMSO, 120°C, 3 h 71%; (ii) $H_2O$/DCM (1:1), 0°C, 1–3 h, 32%–93%. (iii) $K_2CO_3$, $N_2$, DMF; rt., 3–6 h, 5%–74%.

The alternative starting material, *N*-[4-(benzo[d]thiazol-2-yl) phenyl]-2-bromoacetamide (**8**), was synthesized through a three-step process. In the initial step, 2-aminobenzenethiol underwent cyclocondensation with 4-nitrobenzaldehyde, catalyzed by $NH_4Cl$ in DMSO at 120°C for 8 h yielding the corresponding 2-(4-nitrophenyl) benzo[d]thiazole (**6**) in high yield. The subsequent step involved the reduction of the nitro compound (**6**) by tin (II) chloride in absolute ethanol under a nitrogen atmosphere providing 4-(benzo[d]thiazol-2-yl)aniline (**7**) following a reported procedure.[49] The third step comprised the preparation of *N*-[4-(benzo[d]thiazol-2-yl)phenyl]-2-bromoacetamide (**8**) from 4-(benzo[d]thiazol-2-yl)aniline (**7**), using bromoacetyl bromide instead of chloroacetyl chloride, following a reported procedure [50] with notable advantages, including a shorter reaction time (30 min) and excellent yields (99%). Ultimately, compounds **KC21-KC36** were synthesized through the reaction between *N*-[4-(benzo[d]thiazol-2-yl)phenyl]-2-bromoacetamide (**8**) and the Knoevenagel compounds **KC21-KC36 (d)** utilizing anhydrous $K_2CO_3$ as a base in DMF at 70°C for 12–24 h. The structural elucidation of the final compounds (**KC10–KC13** and **KC21–KC36**) was confirmed by FT-IR, $^1$H NMR, $^{13}$C NMR, and mass spectrometry. Similarly, the intermediate compounds **KC10–KC13 (b)**, **6**, and **KC21–KC36 (d)** were characterized by FT-IR analysis. Moreover, the new compounds and key compounds in the outlined synthetic approach (**3**, THZ, **7**, and **8**) underwent further characterization through $^1$H-NMR. The FT-IR spectra of the synthesized compound 4-(benzo[*d*]thiazol-2-yl)-2-methoxyphenol (**3**) displayed characteristic peaks at $\upsilon$ $cm^{-1}$ 3099–2836 (-CH aliphatic and aromatic) with a broad peak corresponding to hydroxy (-OH). In the $^1$H NMR spectra, signals at δ 8.02–6.99 ppm indicated the presence of nearby aromatic C-H protons, while signals at δ 6.17 and 3.99 ppm corresponded to the methoxy C-H and hydroxy O-H protons, respectively. The FT-IR spectra of the (**KC10–KC13 (b)**) derivatives exhibited characteristic acetamide peaks in the ranges of $\upsilon$ $cm^{-1}$ 3265–3288 (-NH) and 1645–1676 (C=O). The structures of the final compounds (**KC10–KC13**) were elucidated using FT-IR, $^1$H NMR, $^{13}$C NMR, and mass spectrometry. The FT-IR spectra displayed four characteristic peaks at $\upsilon$ $cm^{-1}$ 3223–3375, 1645–1709, 1590–1606, and 1415–1420 were observed for N-H, C=O, C=N stretching, and $CH_3$ bending, respectively. In the $^1$H NMR spectra, signals in the range of δ 6.89–8.09 ppm indicated the presence of aromatic protons. Additionally, three singlets observed at δ 8.66–9.73, 3.83–4.07, and 4.69–5.07 ppm were assigned to acetamide N-H, methoxy O-$CH_3$ protons, and aliphatic methylene groups, respectively. The $^{13}$C NMR spectra exhibited characteristic peaks at δ 167.18–168.62 ppm corresponding to carbonyl groups, 166.05–167.66 ppm due to the imine of benzothiazole, and δ 68.42–70.25 ppm confirming the methoxy ($OCH_3$) group. Additional peaks in the range of δ 56.15–56.39 ppm were attributed to aliphatic methylene groups. Mass spectrometry of the **KC10–KC13** series revealed *m/z* value peaks corresponding to the molecular masses of the compounds.

Furthermore, we selected **KC12**, which exhibited promising results in in vitro studies, for detailed characterization using 2D-NMR techniques, including DEPT, HSQC, and HMBC. The DEPT, HSQC, and HMBC spectra were utilized to confirm the structure of the target compound, with the key correlations and structural details illustrated in Figures 2–4.

The FT-IR spectra of the synthesized THZ displayed characteristic peaks at $\upsilon$ $cm^{-1}$ 3124 (-NH) and 1735, 1648 (C=O). In $^1$H NMR spectra, two singlets appeared at (8.56, 1H, and 4.01, 2H), which indicated the presence of N-H proton and -$CH_2$-. In contrast, the Knoevenagel compounds (**KC21–KC36 (d)**) exhibited characteristic peaks at $\upsilon$ $cm^{-1}$ 3097–3242 (-NH), 1666–1749 (C=O), with notable evidence of intramolecular hydrogen bonding between the oxygen atom of carbonyl and -NH 2718-2790 (O...H-N). The FT-IR spectrum of compound **6** showed stretching bands at 3107–3065, 1597, 1519, and 1343 $cm^{-1}$ due to aromatic C-H, C=N, and N=O groups, respectively. Compound **7** exhibited peaks at $\upsilon$ $cm^{-1}$ 3447-3186 (-$NH_2$), 1627 (-$NH_2$, bending), and 1604 (C=N). The $^1$H

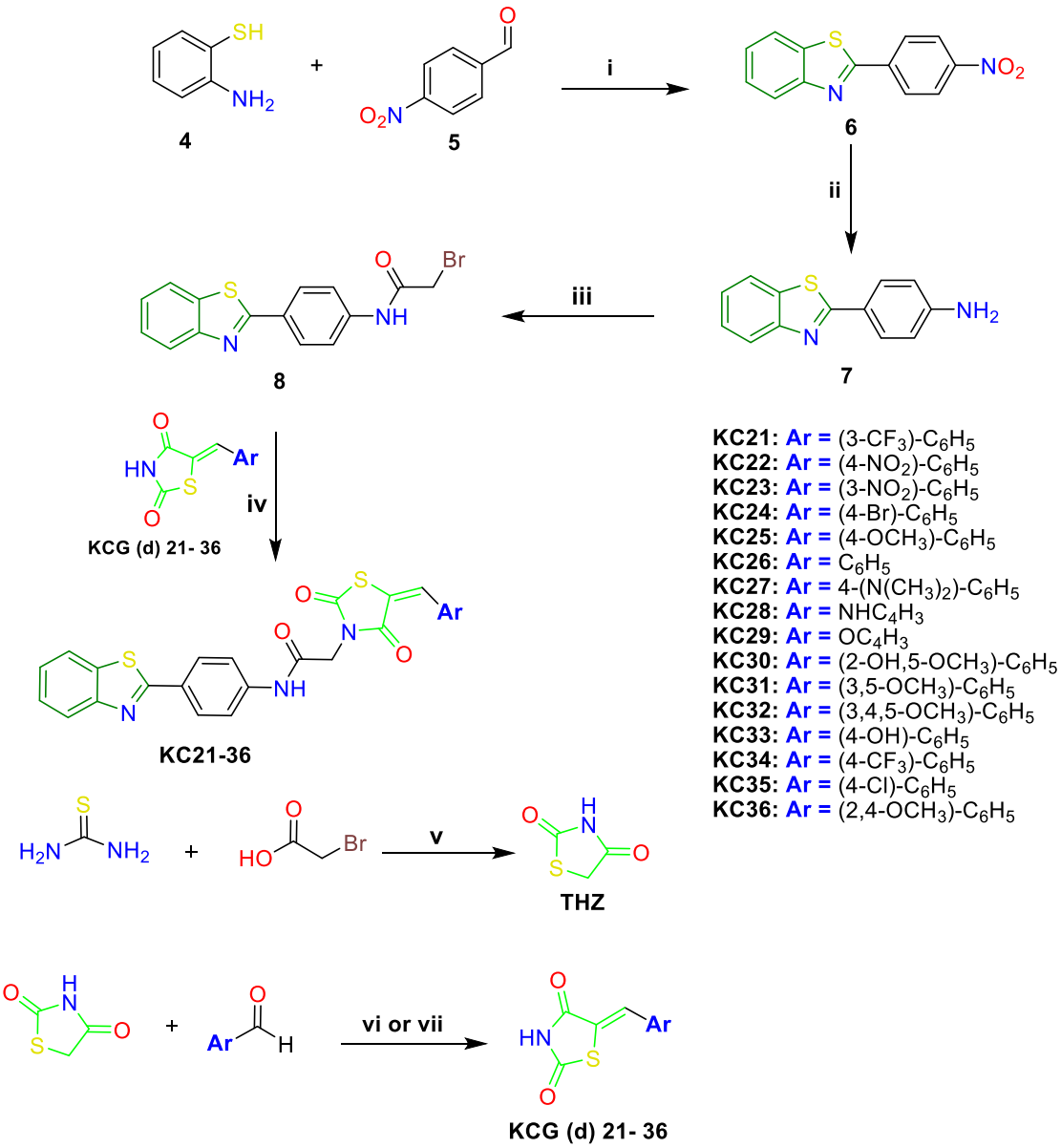


**SCHEME 2** Synthetic route for the preparation of the target compounds **KC21–KC36**. Reagents and conditions: (i) $NH_4Cl$ (4% mol), DMSO, 90°C, 4 h, 99%; (ii) $SnCl_2$, EtOH, $N_2$, reflux, 8 h, 83%; (iii) 1. $K_2CO_3$, $CH_2Cl_2$; 2. 2-Bromoacetyl bromide, 10°C, 1 h, 95%; (iv) $K_2CO_3$, DMF, 70°C, (12–24) h, 15%–93%; (v) HBr, $H_2O$: EtOH (1:4), reflux, 18 h, 69%; method (vi) $CH_3COO\text{-}Na^+$, $CH_3COOH$, reflux, 5–10 h; method (vii) 10 mol% tetrabutylammonium bromide, 110°C, 15–30 min, 19%–92%.

NMR spectra displayed a broad singlet at 3.99 ppm (2H, $NH_2$, $D_2O$ exchangeable), confirming its successful synthesis. The FT-IR spectra of compound **8** revealed characteristic stretching bands at around 3311 and 1669 $cm^{-1}$ for N-H and C=O groups of acetamide, respectively. In the $^1H$ NMR spectra of this compound, a singlet appeared at around δ 8.30 ppm, indicating the presence of an N-H proton. Another characteristic singlet for the two $CH_2$ protons of acetamide appeared at around δ 4.04 ppm, verifying the successful synthesis of the compound. The compounds in the series **KC21–KC36** exhibited characteristic FT-IR stretching bands at $\upsilon$ $cm^{-1}$ 3185–3375 for N-H and 1666–1681 for the C = O groups of acetamide.

Two additional stretching peaks in the range of 1750 to 1682 $cm^{-1}$ were observed, attributed to the two carbonyl groups of THZ. In the $^1H$ NMR spectra, signals in the range of δ 7.38–8.11 ppm indicated the presence of aromatic protons, and three singlets at around δ 10.68–10.83, 7.79–8.17, and 4.49–4.58 ppm represented the acetamide N-H, benzylidene C-H protons, and aliphatic methylene groups, respectively. The $^{13}C$ NMR spectra showed four characteristic peaks at δ 163–172 ppm corresponding to three carbonyl groups and the imine of benzothiazole, and δ 132–135 ppm confirmed the benzylidene (=C-H) group, while other characteristic peaks in the range of δ 43.70–44.86 ppm indicated aliphatic methylene groups. Mass

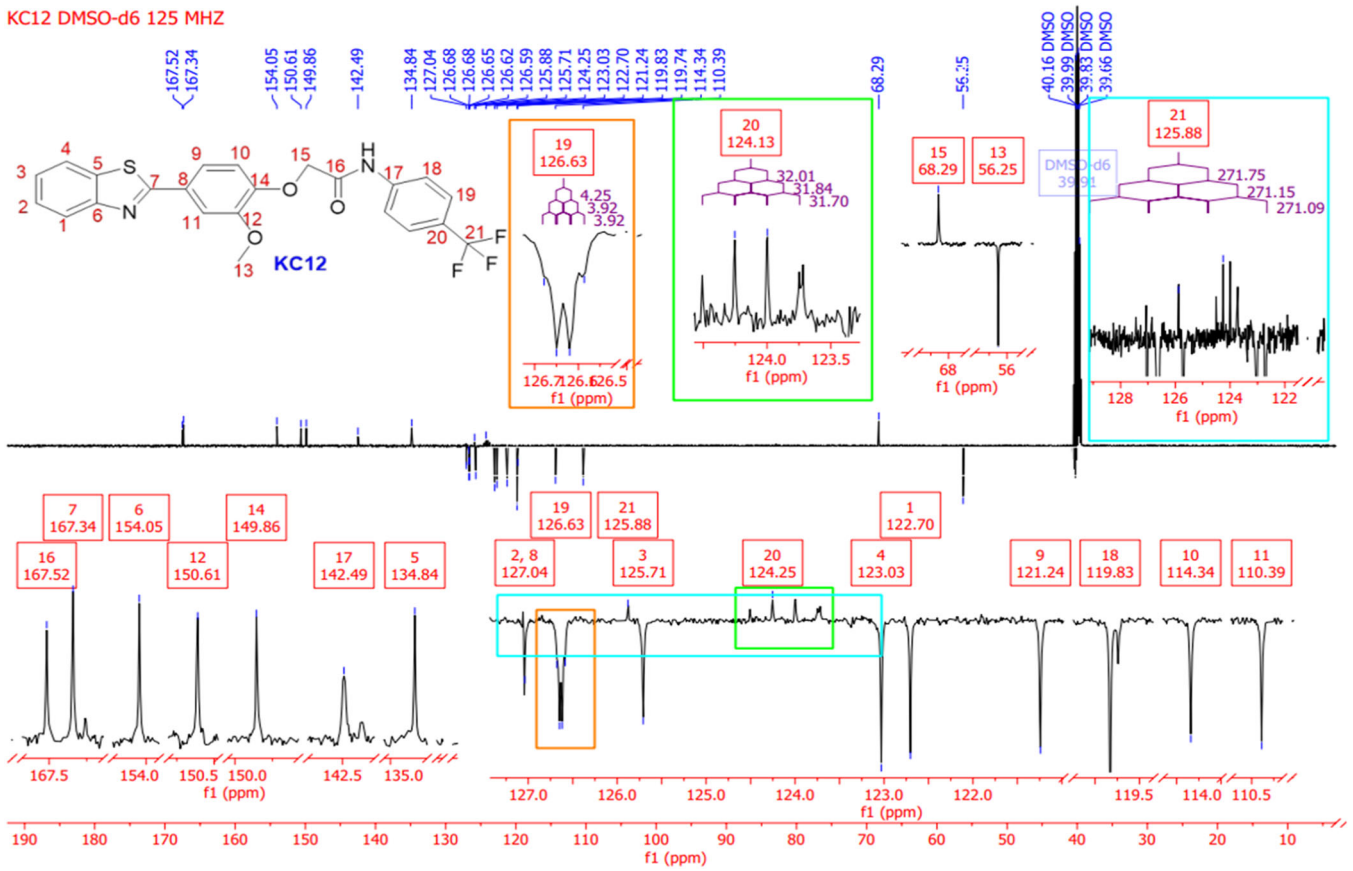


**FIGURE 2** DEPT spectrum of compound **KC12**.

spectra of the **KC21–KC36** series revealed *m/z* value peaks corresponding to the molecular mass of the compounds.

We selected the target compound **KC21** which exhibited promising results in in vitro studies for in-depth characterization using 2D-NMR techniques including DEPT, HSQC, and HMBC. These NMR spectra were instrumental in confirming the structure of the target compound, with key correlations and structural details illustrated in Figures 5–7.

Based on the comprehensive analysis of the FT-IR, $^{1}$H NMR, $^{13}$C NMR, and mass spectra for compounds **KC10–KC13** and **KC21–KC36**, the structures were verified through rigorous spectral analysis (Supporting Information S2, pages 6–67).

## 2.2 | In silico studies

### 2.2.1 | In silico evaluation of physicochemical properties of the newly synthesized compounds

To evaluate the physicochemical descriptors and pharmacologically relevant properties of the synthesized compounds, we utilized the QikProp of Maestro. A comprehensive summary of these properties is presented in Table 1. The molecular weight of the compounds ranged from 420.482 to 561.626, aligning with that of 95% of known drugs. Lipophilicity (Log *p*) values ranged from 3.79 to 5.71, with **KC11** displaying the highest lipophilicity while **KC12** being less lipophilic. The aqueous solubility (QPlogS) values ranged from −8.01 to −5.03, with 6 out of 20 compounds falling outside the recommended range for known drugs. Predicted $IC_{50}$ values for HERG K+ channel blockade ranged from −5.96 to −7.90, with **KC11** having the lowest value and **KC10** the highest. Skin permeability (QPlogKp) values are generally predicted within an acceptable range. The compounds exhibited an optimal number of hydrogen bonding donors and acceptors. QPPCaco values ranged from 114.79 to 3216.84, with **KC12** and **KC13** having the highest values and **KC22** the lowest at 114.79.

We also evaluated the brain penetration properties of the compounds. QPlogBB, representing the brain/blood partition coefficient, ranged from −1.85 to 0.076, within the recommended range. Notably, all compounds were found to have high oral absorption rates, ranging from 100% to 74%, with compounds **KC10**, **KC12**, **KC13**, **KC26**, **KC28**, **KC29**, and **KC36** showing 100% absorption. Since low solubility limits absorption and may lead to low oral bioavailability, a drug with high oral bioavailability potentially reduces the administered dose needed to achieve the desired pharmacological effect, minimizing the risk of side effects and toxicity.[51–53] Based on these predictions, the synthesized compounds exhibit high oral bioavailability. In general, all synthesized compounds align with acceptable ranges or recommended values for 95% of known drugs.

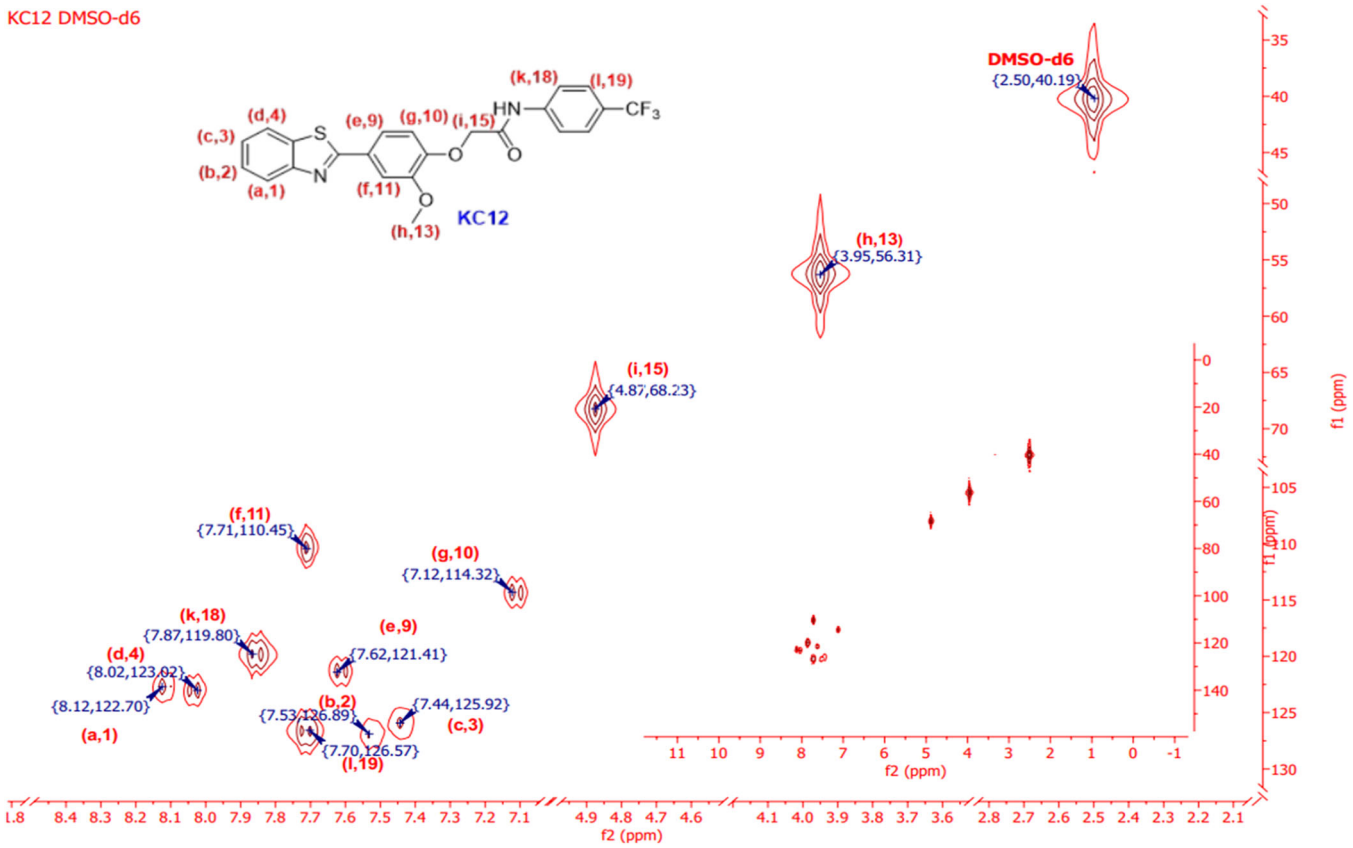


**FIGURE 3** HSQC spectrum of compound **KC12**.

## 2.2.2 | Molecular docking

Molecular docking studies were conducted using AutoDock Vina to explore potential interactions between the newly synthesized compounds and FOXM1 (PDB code: 3G73). All synthesized compounds were subjected to molecular docking within the binding sites of FOXM1-DNA binding domain (DBD) to elucidate their essential interactions with the protein. Based on the molecular docking results of **KC10–KC36** molecules, the binding energies ranged from −6.8 to −5.8 kcal/mol as summarized in Table 2 with the RMSD value (0.000). Notably, compound **KC21** exhibited the strongest binding energy, whereas compound **KC27** displayed the weakest binding energy.

FOXM1 is a transcription factor that harbors a conserved DBD, which recognizes specific consensus sequences within the promoter regions of its target genes.[54] Disrupting the FOXM1-DNA interaction has emerged as a promising therapeutic strategy to inhibit FOXM1's transcriptional activity and hinder cancer cell growth, as supported by preclinical studies.[49] However, translating this approach into clinical applications presents significant pharmacological challenges due to limited knowledge and understanding regarding the pockets for small molecule binding and the presence of a large interaction interface in DBD.[55] These characteristics of FOXM1-DBD make the design of selective and potent FOXM1 inhibitors difficult. Previously published studies indicated that specific residues within the DBD, including Asn-283, Arg-286, and His-287, are highly conserved and contribute significantly to FOXM1 protein and DNA interactions[24,56–59] and targeting these conserved residues through small molecule design offers a potential avenue to develop highly effective FOXM1 inhibitors.

Analysis of the interactions within the FOXM1-DBD and **KC12** complex (Figure 8a) revealed Asn283, His287, and Arg286 as the key amino acid residues (Figure 8b). These residues participated in critical interactions with the **KC12** ligand and formed hydrogen bonds, while Arg286 exhibited additional pi–alkyl and van der Waals interactions. Notably, His287 also participated in a pi–pi T-shaped interaction with the ligand. Interestingly, compared to the previously published FOXM1 inhibitor FDI-6, **KC12** displayed a distinct binding mode (Figure 8c), suggesting that this specific coordination pattern might be more effective for FOXM1-DBD inhibition as evidenced by the in vitro data.

Detailed analysis of the FOXM1-DBD-KC21 complex (Figure 9a) indicated Asn283, His287, and Arg286 as critical residues interacting with the **KC21** ligand (Figure 9b). Specifically, hydrogen bond formation was observed with Asn283, Arg286, and Trp308. Additionally, Leu291 and Leu259 exhibited pi–alkyl interactions, while His287 engaged in a pi–pi T-shaped interaction with the ligand. Furthermore, Arg286 and Trp308 also participated in pi–alkyl and van der Waals interactions with the ligand. In comparison to the standard reference inhibitor, FDI-6 **KC21** displayed a remarkably similar binding mode (Figure 9c). This observation suggests that the specific coordination

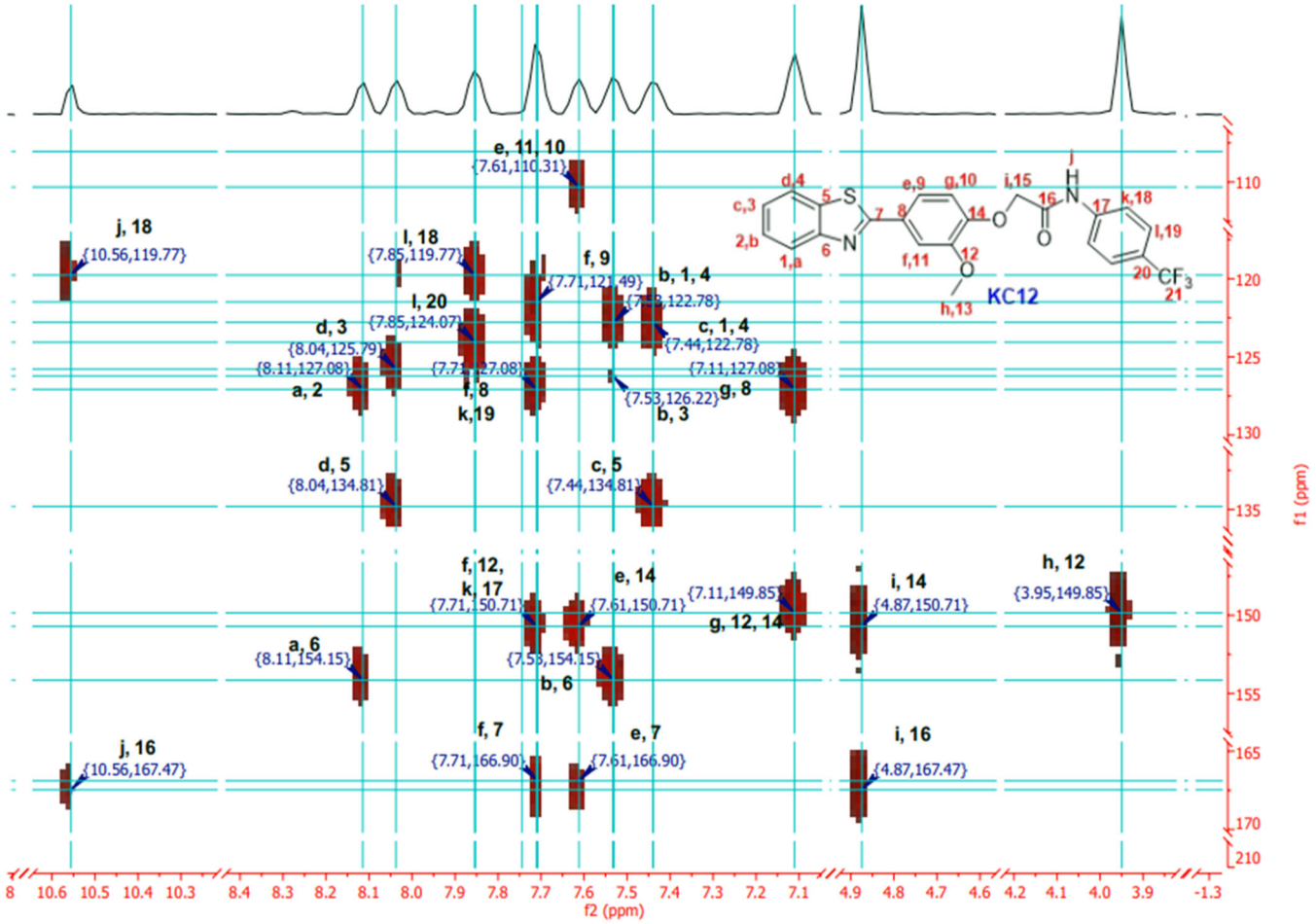


**FIGURE 4** HMBC spectrum of compound **KC12**.

pattern of **KC21** is effective for FOXM1-DBD inhibition, similar to the established mechanism of FDI-6.

The analysis of the FOXM1-DBD-KC30 complex (Figure 10a) interactions has identified Asn283 and Arg286 residues for their significant involvement in this inhibitory mechanism (Figure 10b). Arg286 engages in hydrogen bonding and additional pi–alkyl and van der Waals interactions, while Ser290 also forms hydrogen bonds with the ligand. Furthermore, Leu259 participates in pi–alkyl interactions, and Asn283 is involved in van der Waals interactions with **KC30**. Interestingly, the binding mode of **KC30** is distinct from that of the previously studied FDI-6 (Figure 10c). This unique coordination pattern of **KC30** appears to be more effective in inhibiting FOXM1-DBD as supported by in vitro data.

Docking studies have revealed specific interactions between the ligands **KC12** and **KC30** and the residues within the FOXM1-DBD domain, which may contribute to their enhanced inhibitory efficacy. The unique coordination pattern exhibited by **KC30** and **KC12** (Figures 8 and 10) appears to be particularly effective in inhibiting FOXM1-DBD a finding that is supported by in vitro data. These interactions suggest that the binding mode of **KC30** and **KC12** could serve as a valuable model for the design of more potent FOXM1 inhibitors providing a promising avenue for therapeutic development.

### 2.2.3 | Molecular dynamics simulation

Throughout molecular dynamics (MD) simulation analysis, the compounds exhibited specific interactions with key amino acids. The bar graphs indicated hydrogen bonds, hydrophobic interactions, ionic interactions, and water bridges. According to these results, the phenyl ring of **KC12** directly interacted with Arg286 and Trp308 to generate pi-cation and pi-pi stacking. The amide carbonyl group interacted with Leu259 through water bridges. The methoxy group of phenyls linked to the benzothiazole ring interacted with Arg297 (Figure 11). The most interactions, including H-bonds, hydrophobic, and water bridges, were observed with Arg286 and His287 key residues of FOXM1 for **KC21**. The amide carbonyl group interacted with Asn283 and Ser290 via water bridges. Pi-pi stacking was observed between the His287 residue and phenyl ring linked to the benzothiazole ring (Figure 12). Pi–pi interaction of protein–ligand **KC30** was observed between His287 and benzothiazole ring. These results indicate that the benzothiazole ring of the studied compounds significantly contributes to protein–ligand interactions with key amino acid residues during the 100 ns MD simulations (Figure 13).

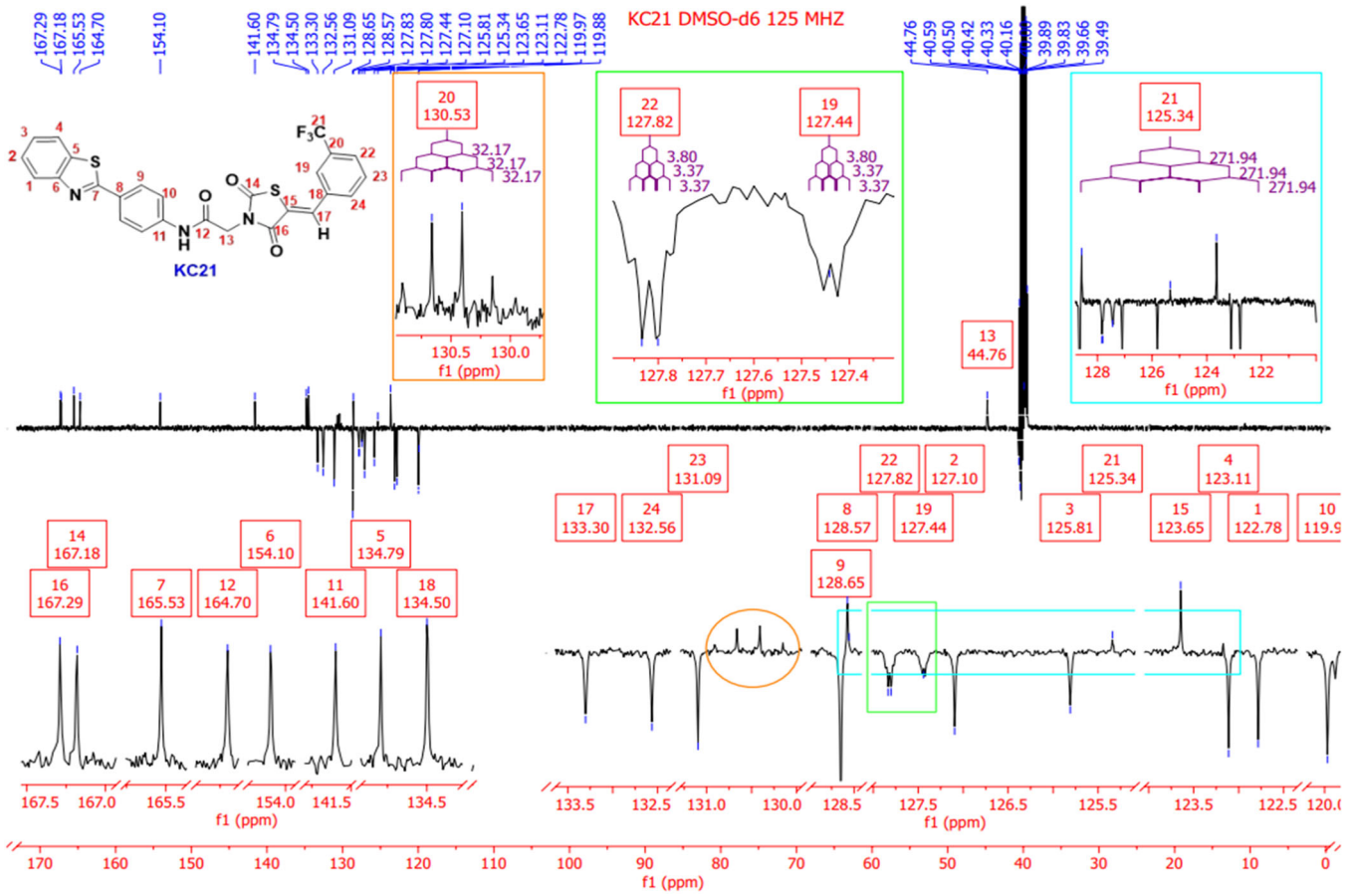


FIGURE 5 DEPT spectrum of compound **KC21**.

## 2.3 | Biological evaluation

### 2.3.1 | In vitro cytotoxic activity

The effect of the newly synthesized 20 compounds on TNBC MDA-MB-231 cell cytotoxicity was evaluated using the MTT cell viability assay. The cells were exposed to increasing concentrations of the compounds for 72 and 96 h. The results showed that most of the compounds (**KC11**, **KC12**, **KC21**, **KC23**, **KC30**, **KC32**, and **KC35**) showed cytotoxicity on MDA-MB-231 cells between 6 and 16 μM, which were lower than the known inhibitor FDI-6 ($IC_{50}$ = 20.79 ± 4.73 μM) (Table 3).

### 2.3.2 | Western blot analysis

FOXM1 inhibitory activity of the compounds was assessed by Western blot analysis after treating MDA-MB-231 cells. For this purpose, the effects of **KC12**, **KC21**, and **KC30** were evaluated at 96 h of treatment. **KC12** inhibited FOXM1 expression at 10 μM concentration compared to the control DMSO. Both **KC21** and **KC30** inhibited FOXM1 expression at concentrations of 10 and 20 μM in MDA-MB-231 cells compared to the control (DMSO) treatment (Figure 14).

## 2.4 | Structure–activity relationship study

The functional groups of the synthesized compounds and their contributions to in vitro anticancer activity were highlighted in Figure 15. Among **KC10–KC13** compounds, electron-withdrawing trifluoromethyl group at 4-position on phenyl ring increased the cytotoxic activity in MDA-MB-231 cells, and therefore, **KC12** was found more cytotoxic than **KC11** containing 4-nitrobenzyl moiety. Moreover, benzothiazole derivatives bearing 4-morpholinomethylphenyl (**KC10**) and 4-methoxyphenyl (**KC13**) moieties showed cytotoxic activity above >50 μM in the TNBC cell line. Among **KC21–KC36** compounds, **KC21** containing trifluoromethyl group at 3-position on phenyl ring showed more cytotoxicity similar to **KC12**. Although 2-hydroxy-5-methoxy substituted compound **KC30** showed cytotoxic activity more twofold than **KC12**, **KC30** markedly decreased FOXM1 expression level at 10 μM than **KC12**. The synthesized benzothiazole-thiazolidine-2,4-dione derivatives bearing 4-methoxy, 4-bromo, 3-nitro, 4-dimethylamine, 4-trifluoromethyl, 4-hydroxy, phenyl, pyrrole, furan substitutions displayed cytotoxic activity higher concentrations in MDA-MB-231 cells. According to a dose-dependent study, the inhibition of FOXM1 expression started at 10 μM by FDI-6 and **KC21**. As a result, **KC12**, **KC21**, and **KC30** were determined as potential inhibitor candidates of FOXM1 for targeted

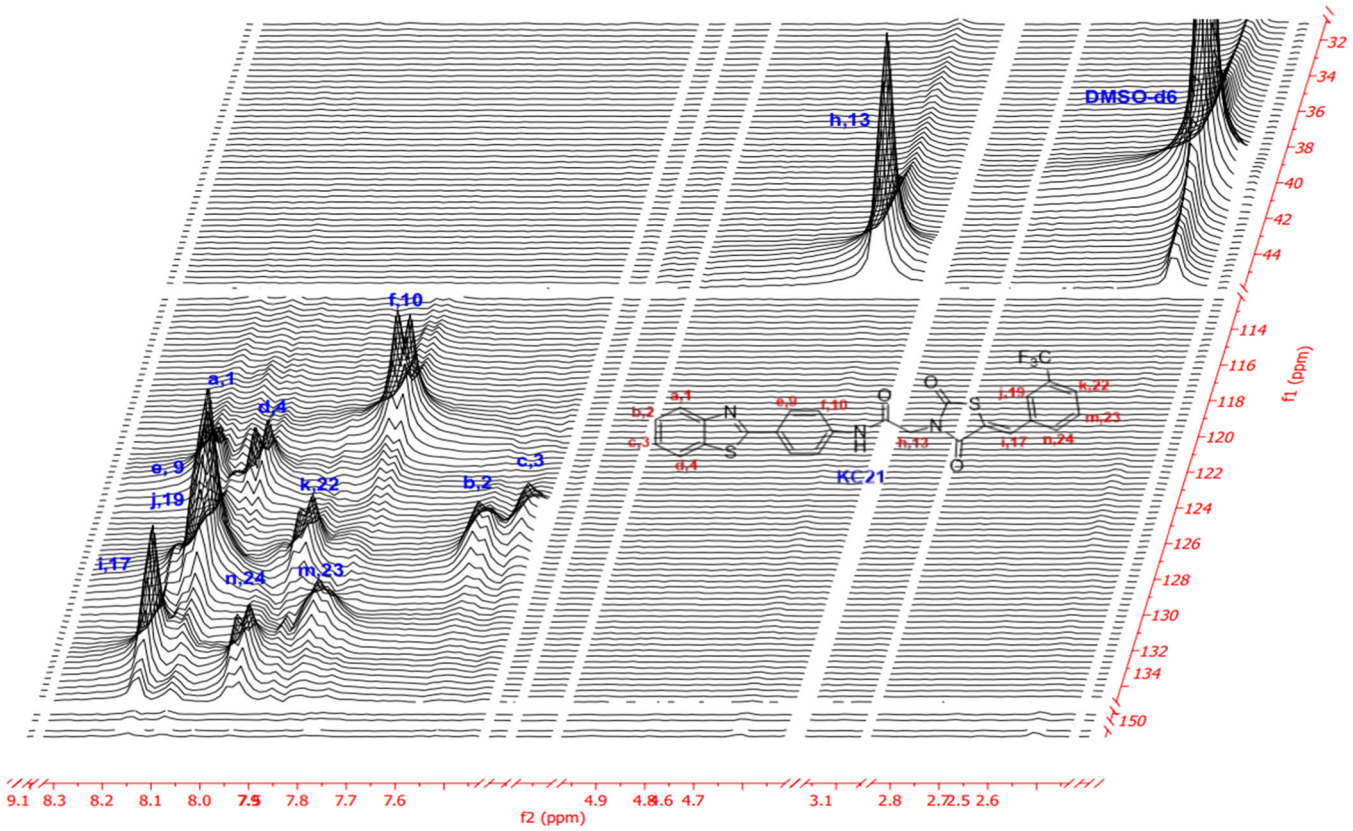


**FIGURE 6** HSQC Stacked plot spectrum of **KC21.**

TNBC therapy. The binding abilities of the synthesized compounds were higher than reference molecule FDI-6. MD simulations supported the interactions with the key amino acids. Thus, these compounds will help in the design of potential candidates.

## 3 | CONCLUSION

In this study, a series of 20 benzothiazole derivatives were synthesized and structurally characterized using various methodologies and evaluated for their antiproliferative activity against MDA-MB-231 cells. The most potent compounds were **KC12**, **KC21**, and **KC30**, and they demonstrated significant antiproliferative activity at $IC_{50}$ values of 6.13, 10.77, and 12.86 μM, respectively. Additionally, **KC12**, **KC21**, and **KC30** were found to inhibit FOXM1 levels in MDA-MB-231 cells. Specifically, **KC21** exhibited notable inhibitor activity at a concentration of 10 μM, while both **KC21** and **KC30** showed strong inhibition at 10 and 20 μM, respectively, compared to control cells. These findings suggest that these benzothiazole derivatives, particularly **KC12**, **KC21**, and **KC30** exhibit FOXM1 better inhibitory activity than commonly used FOXM1 inhibitor FDI-6.

The synthesized compounds were evaluated through molecular docking and MD simulations to explore their interactions with FOXM1's DBD. Docking studies using AutoDock Vina revealed binding energies ranging from −6.8 to −5.8 kcal/mol, with **KC21** showing the strongest binding energy at −6.8 kcal/mol. The key interactions were identified with the residues Asn283, Arg286, and His287, involving hydrogen bonds, pi-alkyl, pi-pi T-shaped, and van der Waals interactions. Compared to the standard inhibitor FDI-6, compounds **KC12**, **KC21**, and **KC30** exhibited distinct and effective binding modes, with **KC12** and **KC30** showing unique coordination patterns and **KC21** mirroring FDI-6's binding mode. MD simulations supported these findings, highlighting stable interactions over 100 ns with key residues like Arg286, His287, and Trp308. Biologically, **KC12**, **KC21**, and **KC30** demonstrated significant inhibitory effects on the proliferation of MDA-MB-231 cells and reduced FOXM1 expression more effectively than FDI-6. Overall, these results suggest that the synthesized compounds, especially **KC12**, **KC21**, and **KC30** are potent FOXM1 inhibitors, warranting further development as therapeutic options.

Notable small molecules such as RCM-123 and Honokiol have been reported to inhibit FOXM1 through a FOXM1 autoregulation loop, albeit requiring extremely high concentrations (approximately 50 μM) to achieve efficacy in vitro.[59–64] Conversely, the chemical probe FDI-6 has been discovered and validated as a specific inhibitor of FOXM1 by directly interfering with the FOXM1-DBD/DNA interaction, providing a unique tool for investigating FOXM1 functions.[57,65,66] STL001 and STL427944, FOXM1 inhibitors, effectively suppress FOXM1 transcriptional activity, presenting promising therapeutic strategies for cancer treatment targeting FOXM1. STL001, a

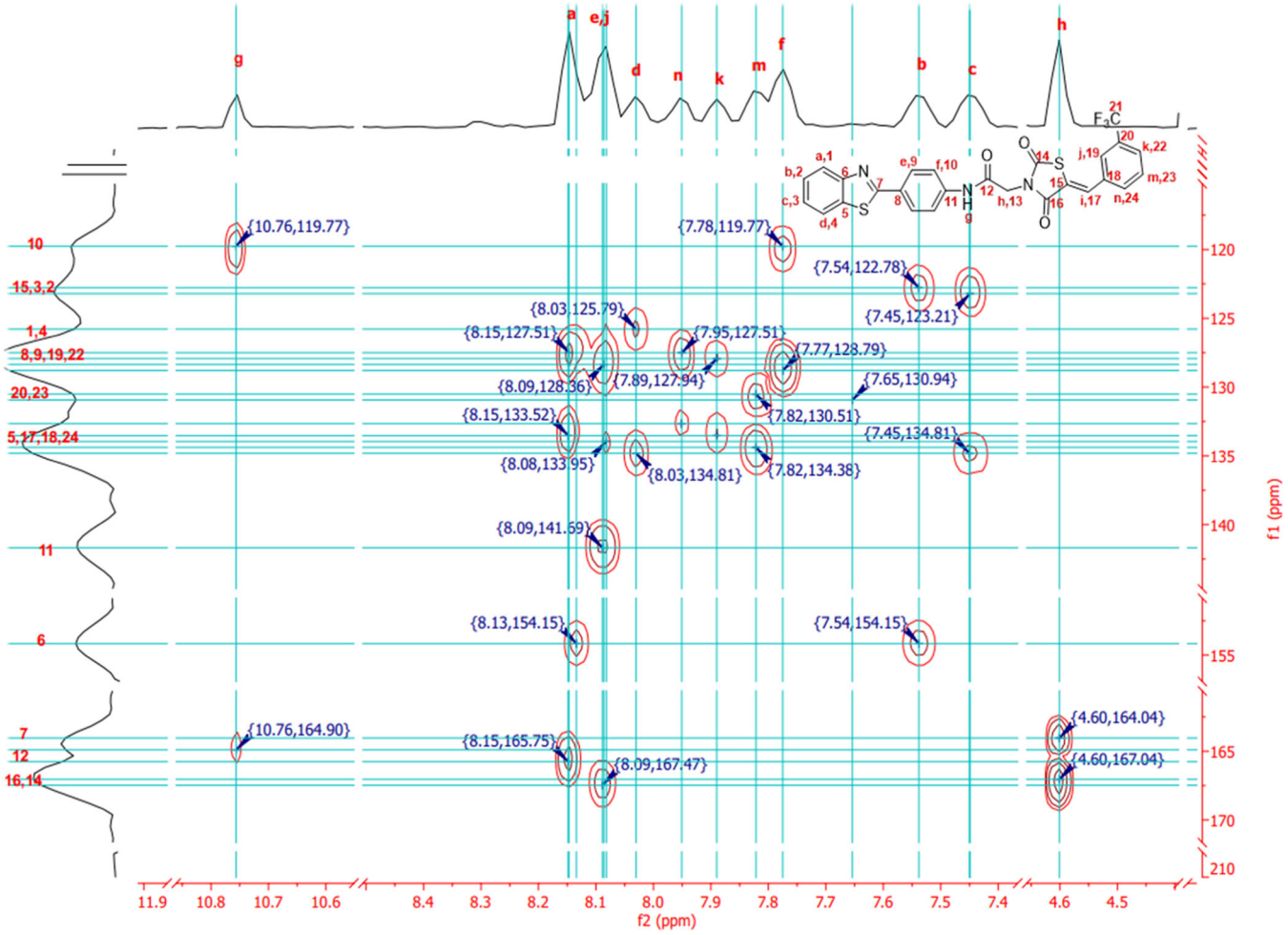


**FIGURE 7** HMBC stacked plot spectrum of **KC21**.

derivative of STL427944, holds potential as a first-generation modification drug for combating tumorigenesis and cancer progression.[67] However, the absence of a FOXM1–ligand co-crystal structure presents challenges for further structure-based optimization of FOXM1 inhibitors.[57]

It is a crucial to highlight that the inhibition of FOXM1 using proteasome inhibitors may pose safety concerns due to their potential to affect multiple signaling pathways and their lack of pharmacological specificity.[60,68–70] Thus, the design of novel and safe FOXM1 inhibitors for clinical application must address these concerns to ensure their successful clinical translation and approval.

The development of FOXM1 inhibitors will also enhance our understanding of FOXM1's role in breast cancer and other malignancies, potentially paving the way for more effective targeted therapies aimed at improving patient outcomes. Further research is necessary to assess the therapeutic efficacy of our new FOXM1 inhibitors in TNBC tumor models and to elucidate the specific mechanisms by which FOXM1 contributes to tumorigenesis across various cancers. This will be essential for the development of more effective treatment strategies.

## 4 | EXPERIMENTAL

### 4.1 | Chemistry

#### 4.1.1 | General

Melting points (°C) were recorded using an X-4 Melting Point Device. IR spectra were measured on a Perkin Elmer Spectrum 100 FT-IR spectrometer. $^{1}$H-NMR and $^{13}$C-NMR spectra (see the Supporting Information S2) were obtained using a JEOL ECX-400 Nuclear Magnetic Resonance Spectrometer, Varian Mercury 500 MHz High-Performance Digital FT-NMR spectrometer and Agilent 600 MHz NMR spectrometer. The following abbreviations are used: (s), singlet; (d), doublet; (t), triplet; (m), multiplet; (q), quartet; (br), broad. Mass spectra were performed using LC-MS/MS analysis (Model: SHIMADZU LC-MS/MS-8040). Chemicals and reagents were sourced from Merck, Sigma-Aldrich, abc, VWR, and other commercial suppliers.

The InChI codes of the investigated compounds, together with some biological activity data, are provided as Supporting Information S1.

DPhG Arch Pharm
Archiv der Pharmazie



**TABLE 1** Molecular descriptors of benzothiazole/benzothiazole thiazolidine-2,4-dione derivatives.

| Compd. No. | mol MW[a*] (130.0–725.0) | QPlogPw[b*] (4.0–45.0) | QPlogPo/w[c*] (−2.0 to 6.5) | QPlogS[d*] (−6.5 to 0.5) | QPlogHERG[e*] (concern below −5) | QPPCaco[f*] (<25 poor, >500 great) | QPlogBB[g*] (−3.0 to 1.2) | QPlogKp[h*] (−8.0 to −1.0) | QPlogKhsa[i*] (−1.5 to 1.5) | P.H.O.A.[j*] (>80% is high, <25% is poor) |
|---|---|---|---|---|---|---|---|---|---|---|
| **KC10** | 489.588 | 13.815 | 4.140 | −5.037 | −7.909 | 797.186 | 0.050 | −2.398 | 0.348 | 100.000 |
| **KC11** | 449.480 | 13.368 | 3.795 | −6.012 | −5.962 | 228.386 | −1.531 | −2.201 | 0.296 | 91.383 |
| **KC12** | 458.454 | 10.555 | 5.716 | −7.416 | −7.151 | 3216.84 | 0.076 | −0.492 | 0.783 | 100.000 |
| **KC13** | 420.482 | 11.029 | 4.730 | −6.026 | −7.015 | 3216.84 | −0.263 | −0.367 | 0.494 | 100.000 |
| **KC21** | 539.546 | 12.510 | 5.684 | −7.701 | −7.065 | 1125.50 | −0.366 | −1.357 | 0.827 | 88.925 |
| **KC22** | 516.545 | 13.936 | 3.953 | −6.609 | −7.159 | 114.791 | −1.857 | −3.190 | 0.501 | 74.001 |
| **KC23** | 516.545 | 13.840 | 4.038 | −6.425 | −7.034 | 158.547 | −1.647 | −2.902 | 0.495 | 77.007 |
| **KC24** | 550.444 | 12.622 | 5.262 | −7.397 | −7.212 | 925.285 | −0.557 | −1.479 | 0.716 | 84.928 |
| **KC25** | 501.574 | 13.036 | 4.713 | −6.620 | −7.095 | 925.285 | −0.794 | −1.424 | 0.551 | 94.673 |
| **KC26** | 471.548 | 12.857 | 4.703 | −6.561 | −7.291 | 925.284 | −0.717 | −1.308 | 0.581 | 100.000 |
| **KC27** | 514.616 | 13.223 | 4.933 | −6.914 | −7.035 | 902.070 | −0.811 | −1.508 | 0.650 | 95.762 |
| **KC28** | 460.524 | 14.093 | 4.132 | −6.132 | −6.987 | 668.63 | −0.853 | −1.722 | 0.446 | 100.000 |
| **KC29** | 461.509 | 12.955 | 4.051 | −5.625 | −6.763 | 950.932 | −0.647 | −1.432 | 0.314 | 100.000 |
| **KC30** | 517.573 | 14.995 | 4.185 | −6.178 | −6.902 | 604.384 | −1.047 | −1.765 | 0.389 | 88.274 |
| **KC31** | 531.600 | 13.162 | 4.713 | −6.225 | −6.623 | 1134.29 | −0.714 | −1.331 | 0.490 | 96.259 |
| **KC32** | 561.626 | 13.649 | 4.829 | −6.444 | −6.732 | 1134.29 | −0.807 | −1.299 | 0.480 | 96.937 |
| **KC33** | 487.547 | 14.949 | 3.984 | −6.343 | −7.153 | 283.039 | −1.376 | −2.361 | 0.440 | 94.158 |
| **KC34** | 539.546 | 12.562 | 5.702 | −8.16 | −7.223 | 925.285 | −0.471 | −1.548 | 0.843 | 87.504 |
| **KC35** | 505.993 | 12.614 | 5.189 | −7.289 | −7.189 | 925.284 | −0.565 | −1.476 | 0.694 | 84.505 |
| **KC36** | 531.600 | 13.155 | 4.726 | −5.953 | −6.479 | 1352.496 | −0.600 | −1.138 | 0.469 | 100.000 |

*Note*: (a*): Molecular weight of the molecule (130.0–725.0); (b*): Predicted water/gas partition coefficient (4.0–45.0); (c*): Predicted octanol/water partition coefficient (−2.0 to 6.5); (d*): Predicted aqueous solubility, log S. S, in mol $dm^{-3}$, is the concentration of solute in a saturated solution in equilibrium with the crystalline solid (−6.5 to 0.5); (e*): Predicted $IC_{50}$ value for HERG K+ blockade channels, (concern below −5); (f*): Predicted apparent Caco-2-cell permeability in nm/sec. Caco-2 cells are a model for the gut-blood barrier (<25 poor, >500 great); (g*): Predicted brain/blood distribution coefficient (−3.0 to 1.2); (h*): Predicted skin permeability, log $K_p$ (−8.0 to −1.0); (i*): Predicted binding to human serum albumin (−1.5 to 1.5); (j*): Predicted human oral absorption (P.H.O.A.) on a scale of 0%–100%. This feature is useful because they both measure the same feature (>80% is high, <25% is poor). Ranges or recommended values for 95% of known drugs.

**TABLE 2** Binding energy values of the compounds.

| Compound | Docking score (kcal/mol) | Compound | Docking score (kcal/mol) |
|---|---|---|---|
| **KC10** | −6.7 | **KC27** | −5.8 |
| **KC11** | −6.4 | **KC28** | −6.0 |
| **KC12** | −6.3 | **KC29** | −6.2 |
| **KC13** | −6.2 | **KC30** | −6.1 |
| **KC21** | −6.8 | **KC31** | −6.1 |
| **KC22** | −6.2 | **KC32** | −6.5 |
| **KC23** | −6.5 | **KC33** | −6.4 |
| **KC24** | −6.2 | **KC34** | −6.3 |
| **KC25** | −6.5 | **KC35** | −6.3 |
| **KC26** | −6.2 | **KC36** | −6.3 |
| **FDI-6** | −5.6 | | |

### 4.1.2 | Preparation of benzothiazole derivatives KC10-KC13

*Synthesis of 4-(benzo[d]thiazol-2-yl)-2-methoxyphenol (**3**)*

4-Hydroxy-3-methoxybenzaldehyde (0.76 g; 5 mmol) and 2-aminobenzenethiol (530 µL; 5 mmol) were combined in 45 mL of DMSO. The reaction mixture was heated to 120°C for 3 h. Subsequently, the mixture was cooled to room temperature and poured into the ice. The resulting precipitate was filtered, water-washed, and recrystallized from ethanol. Affording the desired product (**3**); (0.88 g) as a yellow solid. Reaction progress and compound purity were monitored via TLC using toluene: ethyl acetate: formic acid (T:E:F) (4:3:1) as a mobile phase. Yield, 71%; M.P. 175–177°C; lit. M.P. 171–173°C[71]; FT-IR υ ($cm^{-1}$): 3099–3005 (C-H), 2934, 2836 (C-H), 1604 (C=N), 1584–1523 (C=C), 1425 (C-H, $CH_3$), 1366 (O-H), 1276, 1256, 1034, and 1011 (C-O); $^1$H-NMR (400 MHz, $CDCl_3$): δ 8.02 (d, *J* = 8.2 Hz, 1H), 7.86 (d, *J* = 7.9 Hz, 1H), 7.71 (d, *J* = 1.9 Hz, 1H), 7.53 (dd, *J* = 8.3, 1.9 Hz, 1H), 7.46 (t, *J* = 7.9 Hz, 1H), 7.35 (t, *J* = 7.5 Hz, 1H), 6.99 (d, *J* = 8.1 Hz, 1H), 6.17 (s, 1H), and 3.99 (s, 3H).

*General procedure for the synthesis of **KC10-KC13 (b)***

A solution of substituted aniline/amine (2.5 mmol) in DCM (4 mL) was treated with an aqueous solution of $K_2CO_3$ (0.55 g; 5 mmol, 5 mL). The mixture was then cooled to 0°C, and a solution of bromoacetyl bromide (520 µL; 2.5 mmol) in DCM (2 mL) was added dropwise. The reaction proceeded for 1 h, and then it was monitored by TLC. The solvent was evaporated, water was added, and the mixture was extracted with DCM (3 × 10 mL). The combined organic phases were dried over anhydrous $Na_2SO_4$ and then evaporated under vacuum. The product was washed with hexane and then diethyl ether, to give the corresponding target compounds (**KC11–KC13 (b)**) as pure compounds. But in the case of (**KC10 (b)**), the purification was performed on a silica column chromatography. The elution process involved a gradient of $CHCl_3$ to $CHCl_3$/MeOH (90:10).

2-Bromo-*N*-[4-(morpholinomethyl) phenyl]acetamide (**KC10 (b)**): White solid; yield, 32%; M.P. 158–160°C. FT-IR υ ($cm^{-1}$): 3265 (N-H), 3078, 3011 (C-H), 2979, 2805 (C-H), 1669 (C=O), 1607 (N-H), 1544–1514 (C=C), 1451, 1414 (C-H, -$CH_2$), 1328, 1260, 1068 and 1007 (C-O), 1248, and 1110 (C-N).

2-Bromo-*N*-(4-nitrobenzyl)acetamide (**KC11 (b)**): White solid; yield, 72% M.P. 134–135°C. FT-IR υ ($cm^{-1}$): 3265 (N-H), 3074, 3011 (C-H), 2955, 2854 (C-H), 1645 (C=O), 1607 (N-H), 1548 (C=C), 1514, 1344 (O=N), 1454, 1420 (C-H, -$CH_2$), and 1110 (C-N).[72]

2-Bromo-*N*-[4-(trifluoromethyl)phenyl]acetamide (**KC12 (b)**): White crystal; yield, 93%; M.P. 157–158°C. FT-IR υ ($cm^{-1}$): 3272 (N-H), 3140–3014 (C-H), 2958 (C-H), 1676 (C=O), 1610 (N-H), 1551–1519 (C=C), 1412 (C-H, -$CH_2$), 1317 (C-F), and 1111 (C-N).[72]

2-Bromo-*N*-(4-methoxyphenyl)acetamide (**KC13 (b)**): Light pink crystal; yield, 85%; M.P. 124–126°C. M.P. lit. 120–121°C.[73] FT-IR υ ($cm^{-1}$): 3288 (N-H), 3096–3023 (C-H), 2957–2834 (C-H), 1655 (C=O), 1602 (N-H), 1524–1509 (C=C), 1464–1412 (C-H, -$CH_2$), 1247, 1029 (C-O), 1179, and 1124 (C-N).

*General procedure for the synthesis of benzothiazole derivatives **KC10–KC13***

A solution of 4-(benzo[d]thiazol-2-yl)-2-methoxyphenol **(3)** (1 mmol) and $K_2CO_3$ (2 mmol) in 5 mL of DMF was stirred at room temperature under $N_2$ atmosphere for 12 min. Subsequently, (**KC10–KC13 (b)**) (1 mmol) was added to the solution and stirred for 3–6 h. The reaction progress was monitored by TLC. After completion, the reaction mixture was diluted with ice-cold water and subjected to extraction with ethyl acetate. The combined organic phases were washed with a saline solution, followed by drying over sodium sulfate, and then evaporation under vacuum. The crude product was crystallized from ethanol. After drying the crystalline solid, the pure product was obtained by washing with diethyl ether.

2-[4-(Benzo[d]thiazol-2-yl)-2-methoxyphenoxy]-*N*-(4-(morpholino methyl)phenyl)acetamide (**KC10**): The obtained product needed further purification by silica gel column chromatography using hexane:ethyl acetate:methanol in ratios of 1:1:0 to 1:2:0.5. White solid; yield, 5%; M.P: 179–180°C. FT-IR υ ($cm^{-1}$): 3223 (N-H), 3081–3020 (C-H), 2969–2818 (C-H), 1676 (C=O), 1590 (C=N), 1521–1420 (C=C), 1415, 1375 (C-H, -$CH_3$, and -$CH_2$), 1275, 1261, 1231, 1035, 1007 (C-O), 1174, 1140, and 1113 (C-N). $^1$H-NMR (500 MHz, DMSO-$d_6$): δ 9.73 (s, 1H), 8.04 (d, *J* = 8.0 Hz, 1H), 7.96 (d, *J* = 8.1 Hz, 1H), 7.62–7.58 (m, 3H), 7.53 (dd, *J* = 8.3, 1.6 Hz, 1H), 7.46 (t, *J* = 7.7 Hz, 1H), 7.39–7.33 (m, 3H), 7.15 (d, *J* = 8.4 Hz, 1H), 5.07 (s, 2H), 3.83 (s, 3H), 3.59–3.55 (m, 4H), 3.27 (s, 4H), 3.07 (t, 2H). $^{13}$C-NMR (150 MHz, DMSO-$d_6$): δ 168.62, 167.66, 154.07, 151.08, 149.90, 138.91, 134.78, 131.90, 129.14, 127.02, 126.28, 125.64, 122.97, 122.67, 121.28, 119.93, 114.01, 110.11, 70.25, 66.55, 62.51, 56.15, and 53.64. LC-MS (*m/z*): 490.150 ($[M + H]^+$ 100.00%).

2-[4-(Benzo[d]thiazol-2-yl)-2-methoxyphenoxy]-*N*-(4-nitrobenzyl) acetamide (**KC11**): White solid; yield, 71%; M.P. 183–184°C. FT-IR υ ($cm^{-1}$): 3346 (N-H), 3082–3048 (C-H), 2985–2847 (C-H), 1651 (C=O), 1599 (C=N), 1515, 1349 (O=N), 1470, 1419 (C=C), 1485, 1419 (C-H, -$CH_3$, and -$CH_2$), 1259, 1220, 1023, and 1007 (C-O), 1171, and 1146

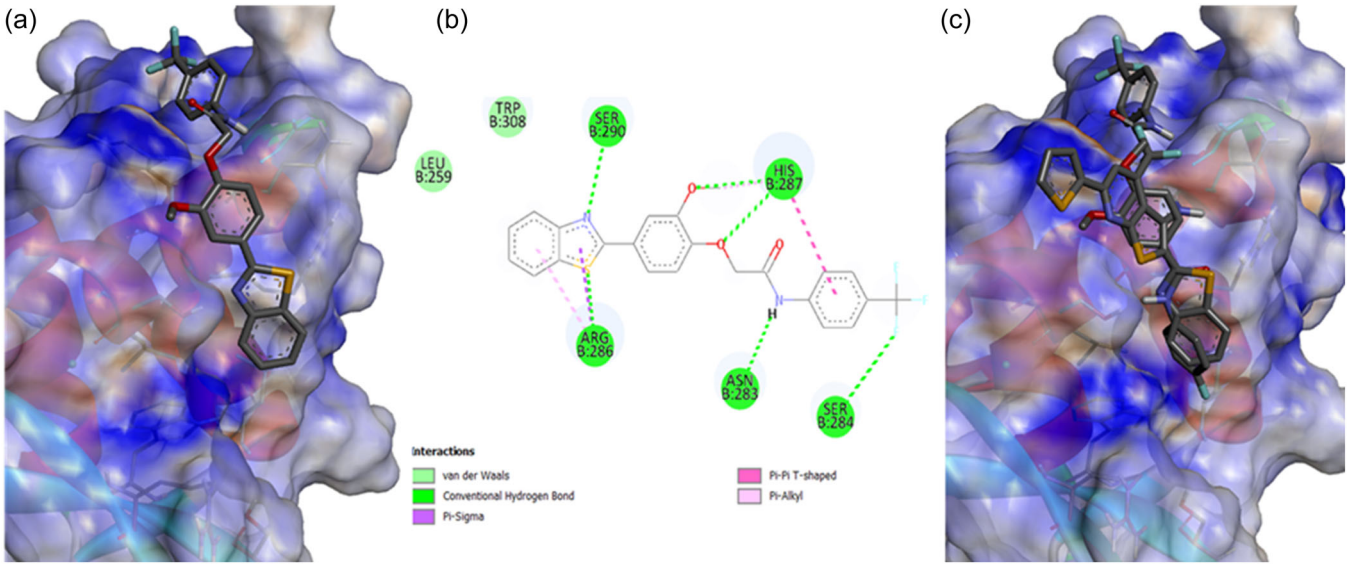


**FIGURE 8** Molecular docking analysis of **KC12** in the FOXM1-DBD binding pocket (PDB ID: 3G73). (a) Stereo view of the docked FOXM1-DBD-KC12 complex. (b) Two-dimensional (2D) illustration of KC12-FOXM1-DBD interactions. (c) Overlay of predicted **KC12** and standard FDI-6 binding modes in FOXM1-DBD active site.

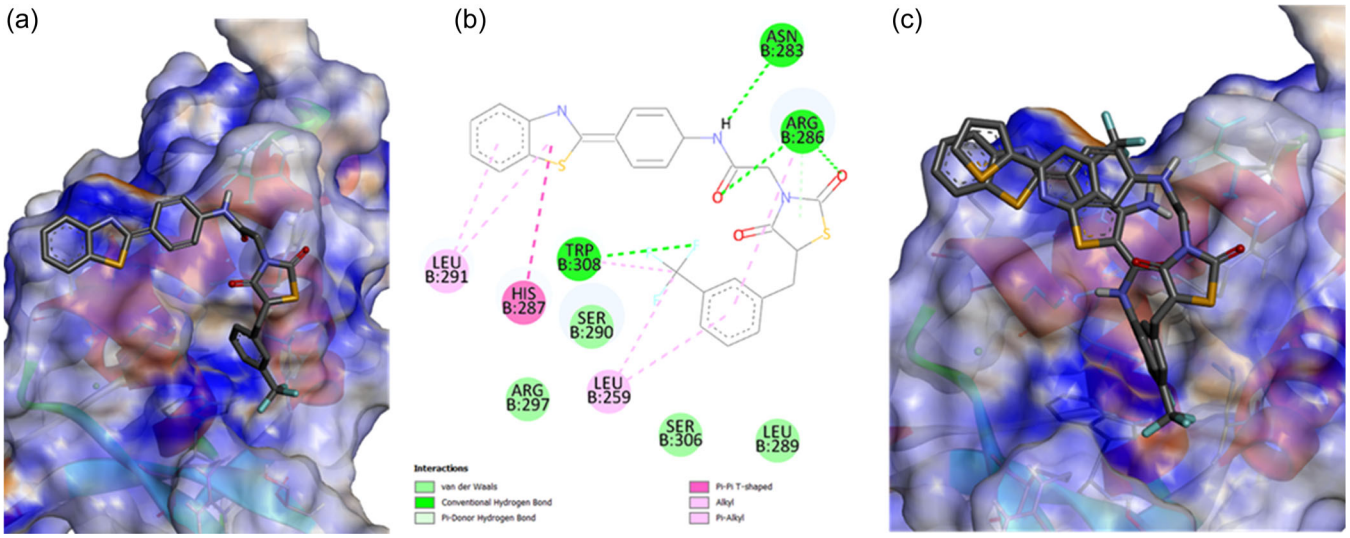


**FIGURE 9** Docking analysis of **KC21** in the FOXM1-DBD binding pocket (PDB ID: 3G73). (a) Stereo view of the docked FOXM1-DBD-KC21 complex. (b) Two-dimensional (2D) illustration of KC21-FOXM1-DBD interactions. (c) Overlay of predicted **KC21** and standard FDI-6 binding modes in FOXM1-DBD active site.

(C-N). $^{1}$H-NMR (400 MHz, DMSO-$d_6$): δ 8.73 (s, 1H), 8.16 (d, $J$ = 8.5 Hz, 2H), 8.09 (d, $J$ = 7.9 Hz, 1H), 8.01 (d, $J$ = 7.9 Hz, 1H), 7.66 (d, 1H), 7.59 (t, $J$ = 7.6 Hz, 1H), 7.51 (d, $J$ = 7.9 Hz, 2H), 7.47–7.33 (m, 2H), 7.05 (d, $J$ = 8.6 Hz, 1H), 4.69 (s, 2H), 4.44 (s, 2H), 3.90 (s, 3H). $^{13}$C-NMR (100 MHz, DMSO-$d_6$): δ 168.42, 167.58, 154.09, 150.54, 149.98, 147.89, 146.96, 134.90, 128.80, 127.13, 125.80, 123.99, 123.10, 122.79, 121.25, 114.56, 110.31, 68.42, 56.25, and 42.08. LC-MS ($m/z$): 450.150 ([M + H]$^+$; 100.00%).

2-[4-(Benzo[d]thiazol-2-yl)-2-methoxyphenoxy]-*N*-(4-(trifluoromethyl)phenyl) acetamide (**KC12**): White solid; yield, 43%; M.P. 170–171°C. FT-IR υ (cm$^{-1}$): 3375 (N-H), 3082–3016 (C-H), 2965–2848 (C-H), 1709 (C=O), 1619 (N-H), 1602 (C=N), 1542, 1519 (C=C), 1485, 1419 (C-H, -$CH_3$, and -$CH_2$), 1329 (C-F), 1266, 1243, 1015, and 1009 (C-O), 1105, and 1066 (C-N). $^{1}$H-NMR (400 MHz, $CDCl_3$): δ 8.99 (s, 1H), 8.04 (dd, $J$ = 8.1, 2.9 Hz, 1H), 7.88 (dd, $J$ = 8.0, 2.9 Hz, 1H), 7.79 (s, 1H), 7.73 (d, $J$ = 7.7 Hz, 2H), 7.64–7.55 (m, 3H), 7.48 (td, $J$ = 7.9, 3.1 Hz, 1H), 7.37 (td, $J$ = 7.7, 3.0 Hz, 1H), 7.02 (dd, $J$ = 8.5, 3.2 Hz, 1H), 4.71 (s, 2H), 4.07 (s, 3H). $^{13}$C-NMR (100 MHz, $CDCl_3$): δ 167.18, 166.71, 154.11, 150.16, 149.24, 140.20, 135.09, 129.46, 126.61

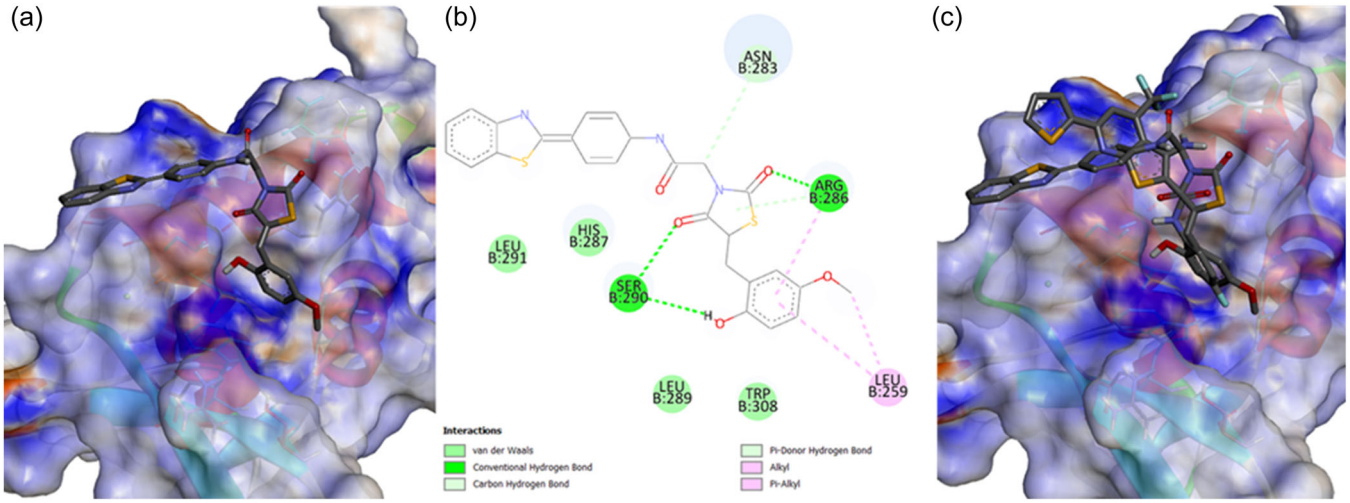


**FIGURE 10** Docking analysis of **KC30** in the FOXM1-DBD binding pocket (PDB ID: 3G73). (a) Stereo view of the docked FOXM1-DBD-KC30 complex. (b) Two-dimensional (2D) illustration of KC30-FOXM1-DBD interactions. (C) Overlay of predicted **KC30** and standard FDI-6 binding modes in FOXM1-DBD active site.

(q, $^{2}J_{CF}$ = 33.2 Hz), 126.53, 126.47, 125.35, 124.10 (q, $^{1}J_{CF}$ = 271.6 Hz), 123.15, 121.72, 121.38, 119.61, 116.01, 110.67, 69.94, and 56.39. LC-MS (*m/z*): 459 ([M + H]$^{+}$ 100.00%).

2-[4-(Benzo[d]thiazol-2-yl)-2-methoxyphenoxy]-*N*-(4-methoxy phenyl)acetamide (**KC13**): White crystal; yield, 62%; M.P. 177–178°C. FT-IR υ (cm$^{-1}$): 3296 (N-H), 3050–3016 (C-H), 2965–2839 (C-H), 1667 (C=O), 1636 (N-H), 1597 (C=N), 1531, 1513 (C=C), 1493–1418 (C-H, -$CH_3$, and -$CH_2$), 1264, 1238, and 1032 (C-O), 1180, and 1125 (C-N). $^{1}$H-NMR (400 MHz, $CDCl_3$): δ 8.66 (s, 1H), 8.04 (d, *J* = 8.1 Hz, 1H), 7.88 (d, *J* = 8.0 Hz, 1H), 7.78 (s, 1H), 7.58 (d, *J* = 8.5 Hz, 1H), 7.54–7.44 (m, 3H), 7.37 (t, *J* = 7.3 Hz, 1H), 7.01 (d, *J* = 7.9 Hz, 1H), 6.89 (d, *J* = 8.5 Hz, 2H), 4.69 (s, 2H), 4.06 (s, 3H), and 3.79 (s, 3H). $^{13}$C-NMR (100 MHz, $CDCl_3$): δ 167.37, 166.05, 156.82, 154.13, 150.09, 149.41, 135.09, 130.20, 129.06, 126.49, 125.29, 123.12, 121.89, 121.72, 121.35, 115.43, 114.33, 110.51, 69.69, 56.36, and 55.56. LC-MS (*m/z*): 421 ([M + H]$^{+}$ 100.00%).

### 4.1.3 | General procedure for the synthesis of KC21–KC36

*Synthesis of thiazolidine-2,4-dione (THZ)*

A solution of thiourea (0.76 g; 10 mmol) in 6 mL distilled water was added to 25 mL of ethanol, followed by the addition of a solution of bromoacetic acid (1 mL; 10 mmol) in 6 mL distilled water. The mixture was stirred at room temperature for approximately 15 min, resulting in the formation of a white precipitate. The concentrated hydrobromic acid (HBr) (6 mL) was then added dropwise until the precipitate disappeared. The reaction mixture underwent reflux for 12 h and was subsequently cooled in an ice bath, leading to the formation of white crystals. The obtained white crystals were collected via suction filtration and washed several times with water to remove excess acid. The crude product was recrystallized from ethanol to afford thiazolidine-2,4-dione (THZ) as a pure product with a good yield. White crystal; yield, 69%; M.P. 126–128°C, lit. M.P. 125.3–127.5°C).[74] FT-IR υ (cm$^{-1}$): 3124 (N-H), 3036–2824 (C-H), 2718 (N-H……O intra-hydrogen bond), 1735 and 1648 (C=O), 1339 (C-H, $CH_2$), 1159 (O=C-N-C=O), 890 (C-S). $^{1}$H-NMR (400 MHz, $CDCl_3$): δ 8.56 (s, 1H), 4.01 (s, 2H).

*Synthesis of 2-(4-nitrophenyl) benzo[d]thiazole (**6**)*

To a solution of 4-nitrobenzaldehyde (0.76 g; 5 mmol) and $NH_4Cl$ (0.11 g; 0.2 mmol; 4 mmol) in DMSO (20 mL), 2-aminobenzenethiol (540 µL; 5 mmol) was added dropwise with stirring. The reaction mixture was then heated to 120°C for 8 h. After cooling to room temperature, the resulting mixture was poured into crushed ice. The formed precipitate was filtered, washed with water, and recrystallized from ethanol. The progress of the reaction and the purity of the compound were monitored by TLC using TEF (4:3:1) as a mobile phase. Yellow solid; yield, 99%; M.P. 228–229°C; lit. M.P. 229–230°C.[75] FT-IR υ (cm$^{-1}$): 3107–3065 (C-H), 1606 (C=N), 1597–1558 (C=C), 1519, and 1343 ($NO_2$).

*Synthesis of 4-(benzo[d]thiazol-2-yl) aniline (**7**)*

According to the reported method,[50] a mixture of 2-(4-nitrophenyl) benzo[*d*]thiazole (**6**) (0.78 g; 3 mmol) and tin(II)chloride (2.4 g; 15 mmol) in ethanol (15 mL) was stirred under nitrogen gas to reflux for 12 h. After evaporation of ethanol, ethyl acetate was added to the residue, and the organic phase was washed with 2 M aqueous NaOH (3 × 30 mL) and water (2 × 30 mL) and dried over $Na_2SO_4$. The solvent was evaporated. The crude product was crystallized from ethanol to give 2-(4-aminophenyl) benzo[**d**]thiazole (**KCG (b)**). The progress of the reaction and the purity of the compound were checked by TLC using TEF (5:4:1) as the mobile phase. Dark yellow solid; Yield, 82%; M.P. 126–128°C; lit. M.P. 125–127°C.[50] FT-IR υ (cm$^{-1}$): 3447 (N-H), 3187–3030 (C-H), 1627 (C=N), 1604 (N-H), 1590–1528 (C=C).

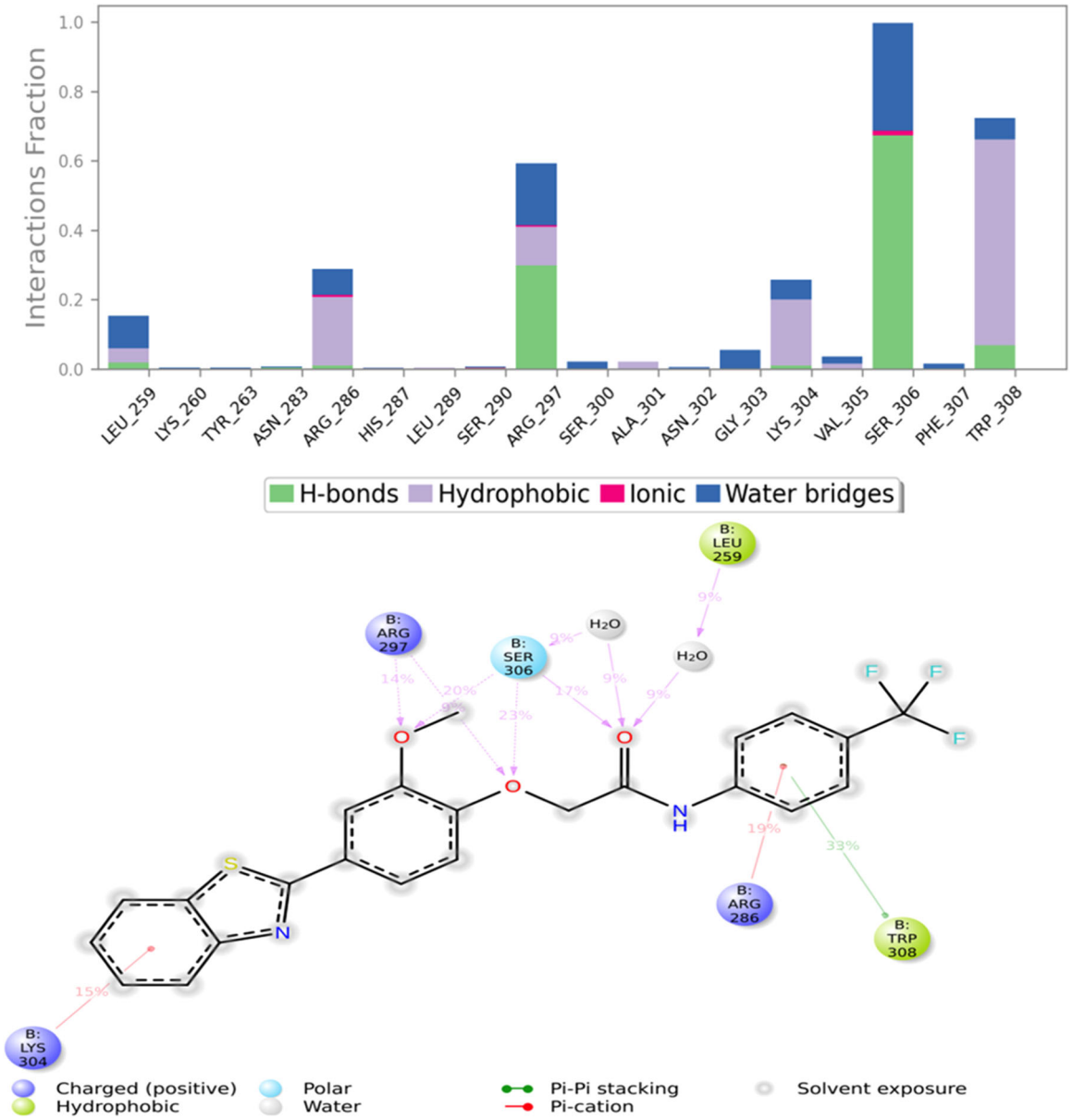


**FIGURE 11** The temporal evolution of interactions between FOXM1-DBD and **KC12** during 100 ns MD simulation. Interactions are classified into distinct categories, including hydrogen bonds, hydrophobic interactions, ionic interactions, and water bridges. The "Interactions Fraction" parameter quantifies the proportion of simulation time during which each specific interaction persists. MD, molecular dynamics.

$^1$H-NMR (400 MHz, $CDCl_3$): δ 7.98 (d, *J* = 8.1 Hz, 1H), 7.89 (d, *J* = 8.1 Hz, 2H), 7.84 (d, *J* = 8.0 Hz, 1H), 7.43 (t, *J* = 7.8 Hz, 1H), 7.31 (t, *J* = 7.6 Hz, 1H), 6.73 (d, *J* = 8.4 Hz, 2H), and 3.99 (br, s, 2H).

*Synthesis of* N-*[4-(benzo[d]thiazol-2-yl)phenyl]-2-bromoacetamide (**8**)*

To a solution of 4-(benzo[*d*]thiazol-2-yl) aniline (**7**) (0,453 g; 2 mmol) in 20 mL $CH_2Cl_2$, anhydrous $K_2CO_3$ (0.125 g; 0.9 mmol; 45 mol%) was added. Subsequently, bromoacetyl bromide (350 µL; 4 mmol) was added dropwise with continuous stirring at 10°C. The reaction mixture was stirred for an additional 30 min. After the evaporation of dichloromethane, the residue was washed several times with water, and the resulting precipitate was collected by suction filtration. The crude product underwent crystallization from methanol. Light brown solid; yield, 99%; M.P. 206–208°C; FT-IR υ ($cm^{-1}$): 3258 (N-H), 3116–3009 (C-H), 2958 (C-H), 1655 (C=O), 1598 (C=N), 1538-1480 (C=C), 1434 (C-H, $CH_2$), 1180 (C-N). $^1$H-NMR (400 MHz, $CDCl_3$): δ 8.30 (s, 1H), 8.08 (d, *J* = 7.9 Hz, 2H), 8.05 (d, *J* = 7.9 Hz, 1H), 7.89 (d, *J* = 8.1 Hz, 1H), 7.69 (d, *J* = 7.9 Hz, 2H), 7.48 (t, *J* = 7.6 Hz, 1H), 7.37 (t, *J* = 7.6 Hz, 1H), and 4.04 (s, 2H).

*General procedure for the synthesis of the Knoevenagel compounds (KC21–KC36 (d))*

Method (vi) in Scheme 2. According to the reported method,[47] Knoevenagel compounds were synthesized through the condensation of aldehydes with thiazolidine-2,4-dione. The synthesis involved

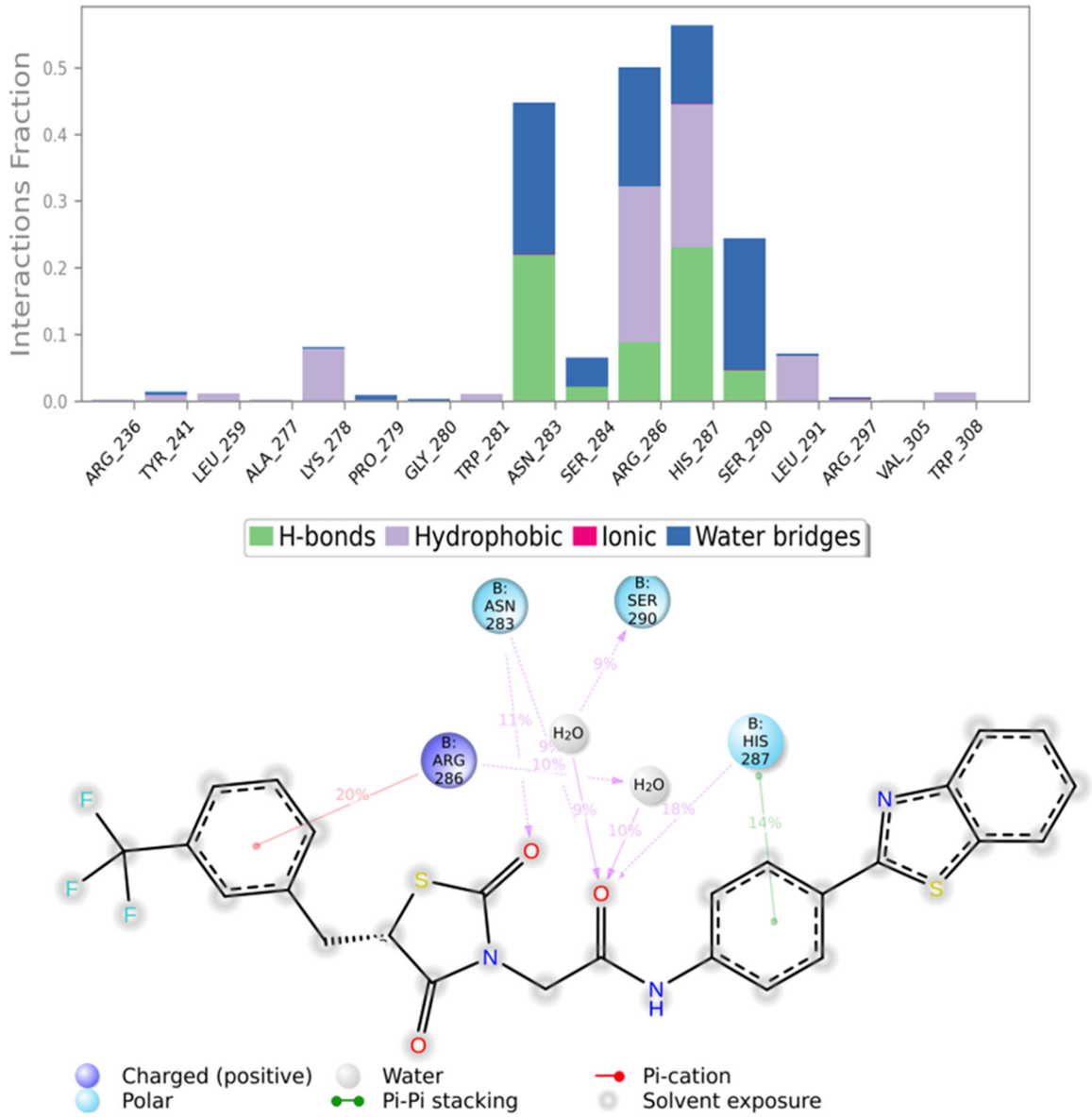


**FIGURE 12** The temporal evolution of interactions between FOXM1-DBD and **KC21** during 100 ns MD simulation. Interactions are classified into distinct categories, including hydrogen bonds, hydrophobic interactions, ionic interactions, and water bridges. The "Interactions Fraction" parameter quantifies the proportion of simulation time during which each specific interaction persists. MD, molecular dynamics.

refluxing thiazolidine-2,4-dione (0.585 g; 5 mmol) with aromatic aldehydes (8.75 mmol) in the presence of sodium acetate (0.031 g; 7.5 mol %). Glacial acetic acid (5 mL) was used as a solvent, and the reaction mixture was refluxed for 5–10 h with stirring. Monitoring of the reaction was performed using TLC with hexane and EtOAc in a 4:1 ratio as the mobile phase. After cooling the reaction mixture, a solid product was obtained, filtered, and washed with water. The crude product was recrystallization from an EtOH:DMF (5:2) mixture.

Method (vii) in Scheme 2. According to the reported method,[48] a mixture of aromatic aldehyde (5 mmol), thiazolidine-2,4-dione (0.585 g; 5 mmol) using 10 mol% tetrabutylammonium bromide (TBAB) as catalyst was condensed at 110°C on oil bath under solvent-free reaction conditions. After completion of the reaction as indicated by TLC, the crude product was cooled, washed with water (10 mL), filtered and recrystallization from a mixture of EtOH/DMF (5:2).

5-[3-(Trifluoromethyl)benzylidene]thiazolidine2,4-dione (**KC21 (d)**): Method vi. Cream solid; yield, 68%; M.P. 156–157°C. lit. M.P. 180–182°C.[76] FT-IR υ ($cm^{-1}$): 3152 (N-H), 3027 (C-H), 2770 (N-H.....O intra hydrogen bond), 1742, 1701 (C=O), 1606 (C=C), 1587, 1431 (C=C), 1327 (C-F), 1287 (C-N), 1156, 1113 (O=C-N-C=O), 902 (C-S).

5-(4-Nitrobenzylidene)thiazolidine-2,4-dione (**KC22 (d)**): Method vi. Yellow solid; yield: 64%; M.P. 259–261°C; M.P. lit. 220–223°C,[77] >250°C.[78] FT-IR υ ($cm^{-1}$): 3191 (N-H), 3084 (C=C-H), 3049–2963 (C-H), 2737 (N-H.....O intra-hydrogen bond), 1751, 1673 (C=O),

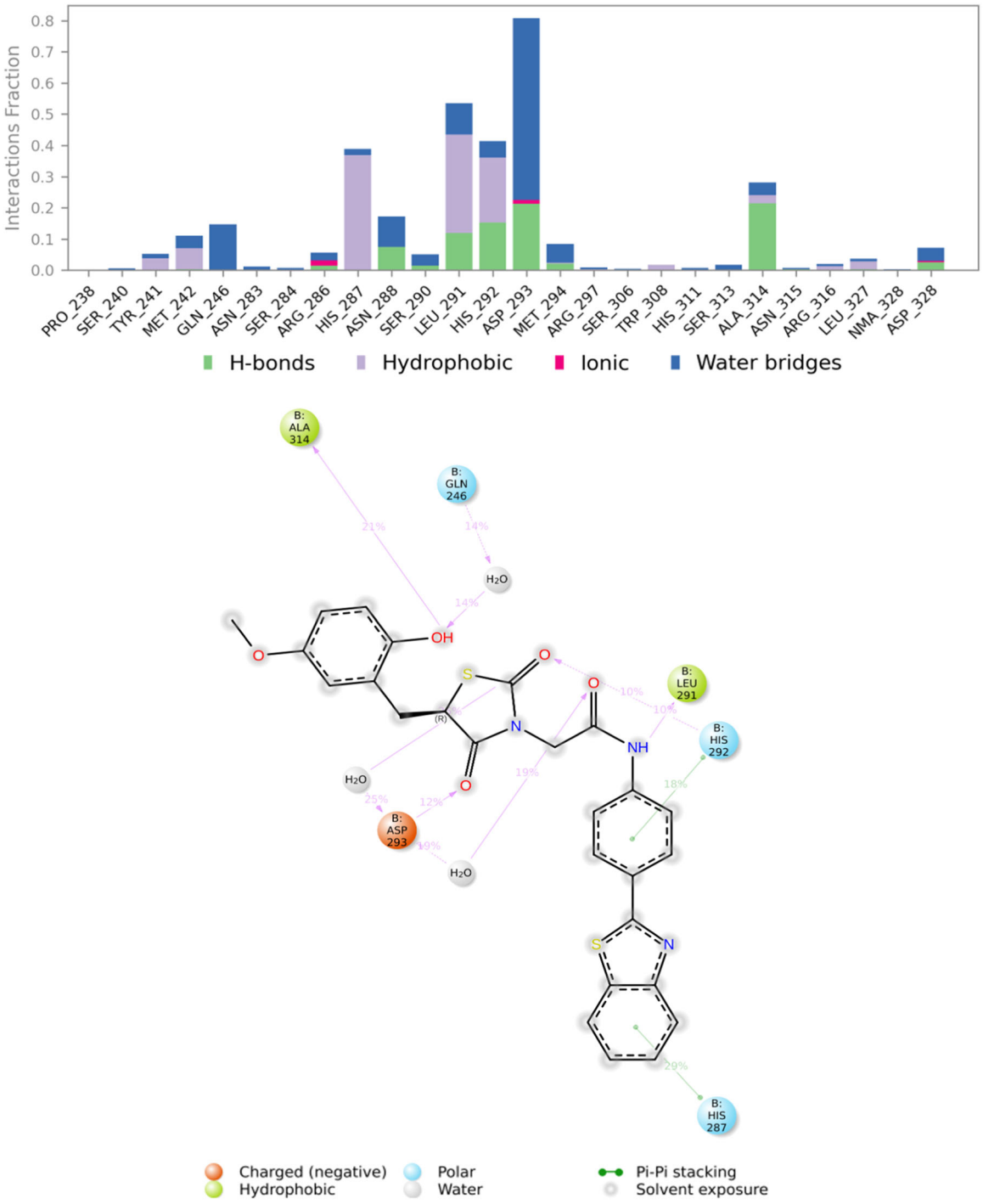


**FIGURE 13** Depicts the temporal evolution of interactions between FOXM1-DBD and **KC30** during 100 ns MD simulation. Interactions are classified into distinct categories, including hydrogen bonds, hydrophobic interactions, ionic interactions, and water bridges. The "Interactions Fraction" parameter quantifies the proportion of simulation time during which each specific interaction persists. MD, molecular dynamics.

1608 (C=C), 1530, 1346 (NO2), 1491–1408 (C=C), 1283 (C-N), 1148, 1110 (O=C-N-C=O), and 904 (C-S).

5-(3-Nitrobenzylidene)thiazolidine-2,4-dione (**KC23 (d)**): Method vii. Yellow solid; yield: 68%; M.P. 184–186°C; lit. M.P. 250°C.[77] FT-IR υ ($cm^{-1}$): 3150 (N-H), 3085 (C=C-H), 3070–3035 (C-H), 2766 (N-H.....O intra-hydrogen bond), 1744, 1688 (C=O), 1606 (C=C), 1528, 1325 ($NO_2$), 1483–1433 (C=C), 1291 (C-N), 1154, 1100 (O=C-N-C=O), and 928 (C-S).

5-(4-Bromobenzylidene)thiazolidine-2,4-dione (**KC24 (d)**): Method vii. Cream solid; yield, 68%; M.P. 265–267°C; lit. M.P. 262–264°C.[79] FT-IR υ ($cm^{-1}$): 3145 (N-H), 3088 (C=C-H), 3053 (Ar C-H), 2766 (N-H.....O intra-hydrogen bond), 1753, 1717 (C=O), 1610 (C=C), 1587, 1573 (C=C), 1282 (C-N), 1154, 1066 (O=C-N-C=O), and 897 (C-S).

5-(4-Methoxybenzylidene)thiazolidine-2,4-dione (**KC25 (d)**): Method vii. Light yellow solid; yield, 19%; M.P. 222–223°C. lit. M.P.

**TABLE 3** In vitro $IC_{50}$ values of the compounds.

| Compound | Compound structure | $IC_{50}$ (μM) | Compound | Compound structure | $IC_{50}$ (μM) |
|---|---|---|---|---|---|
| **KC10** | 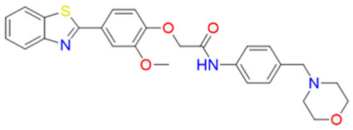 | >50 | **KC27** | 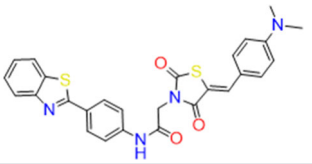 | >50 |
| **KC11** | 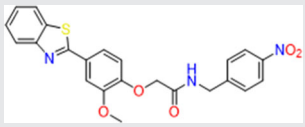 | 15.58 ± 3.45 | **KC28** | 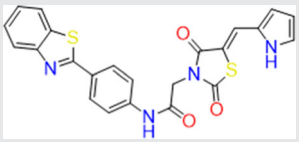 | 41.73 ± 4.58 |
| **KC12** | 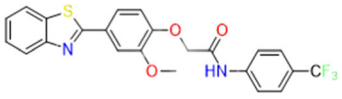 | 6.13 ± 4.82 | **KC29** | 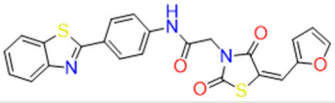 | 38.43 ± 4.70 |
| **KC13** | 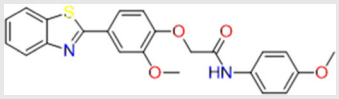 | >50 | **KC30** | 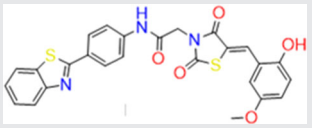 | 12.86 ± 3.61 |
| **KC21** | 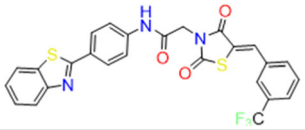 | 10.77 ± 3.85 | **KC31** | 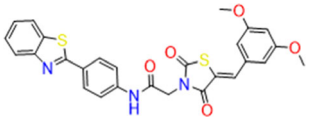 | 35.18 ± 6.59 |
| **KC22** | 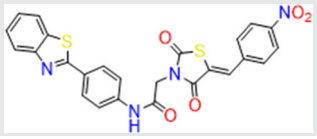 | >50 | **KC32** | 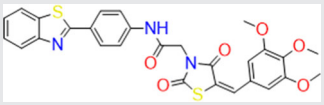 | >50 |
| **KC23** | 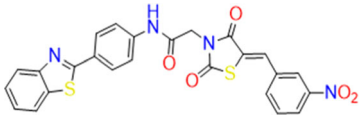 | 10.95 ± 2.33 | **KC33** | 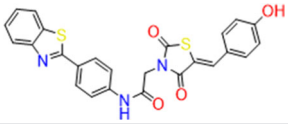 | 42.96 ± 6.19 |
| **KC24** | 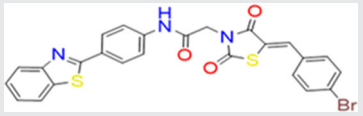 | >50 | **KC34** | 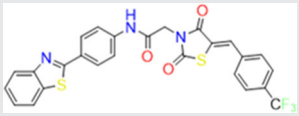 | >50 |
| **KC25** | 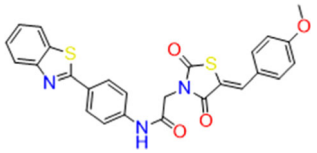 | >50 | **KC35** | 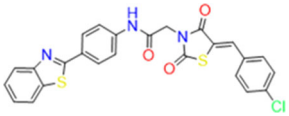 | 15.34 ± 4.02 |
| **KC26** | 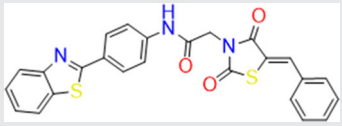 | >50 | **KC36** | 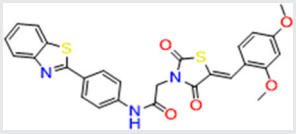 | >50 |
| **FDI-6** | 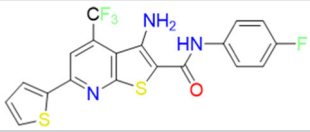 | 20.79 ± 4.73 | | | |

*Note*: $IC_{50}$ values determined in triplicates are presented as mean ± SEM, $n = 3$. Data analysis and $IC_{50}$ determination were performed with GraphPad Prism.

210–212°C,[77] 216–218°C.[48] FT-IR υ ($cm^{-1}$): 3242 (N-H), 3106 (C=C-H), 3009–2965 (C-H), 2839 (C-H -$CH_3$), 2777 (N-H.....O intra-hydrogen bond), 1754, 1690 (C=O), 1595 (C=C), 1507–1445 (C=C), 1345 (C-H, -$CH_3$), 1300, 1015 (C-O), 1251 (C-N), 1155, 1140 (O=C-N-C=O), 911 (C-S).

5-Benzylidenethiazolidine-2,4-dione (**KC26 (d)**): Method vi. Cream solid; yield, 30%; M.P. 243–245°C. lit. M.P. 240°C.[79] FT-IR υ ($cm^{-1}$): 3143 (N-H), 3018 (C-H), 2787 (N-H.....O intra-hydrogen bond), 1739, 1686 (C=O), 1608 (C=C), 1505, 1447 (C=C), 1276 (C-N), 1156, 1143 (O=C-N-C=O), and 920 (C-S).

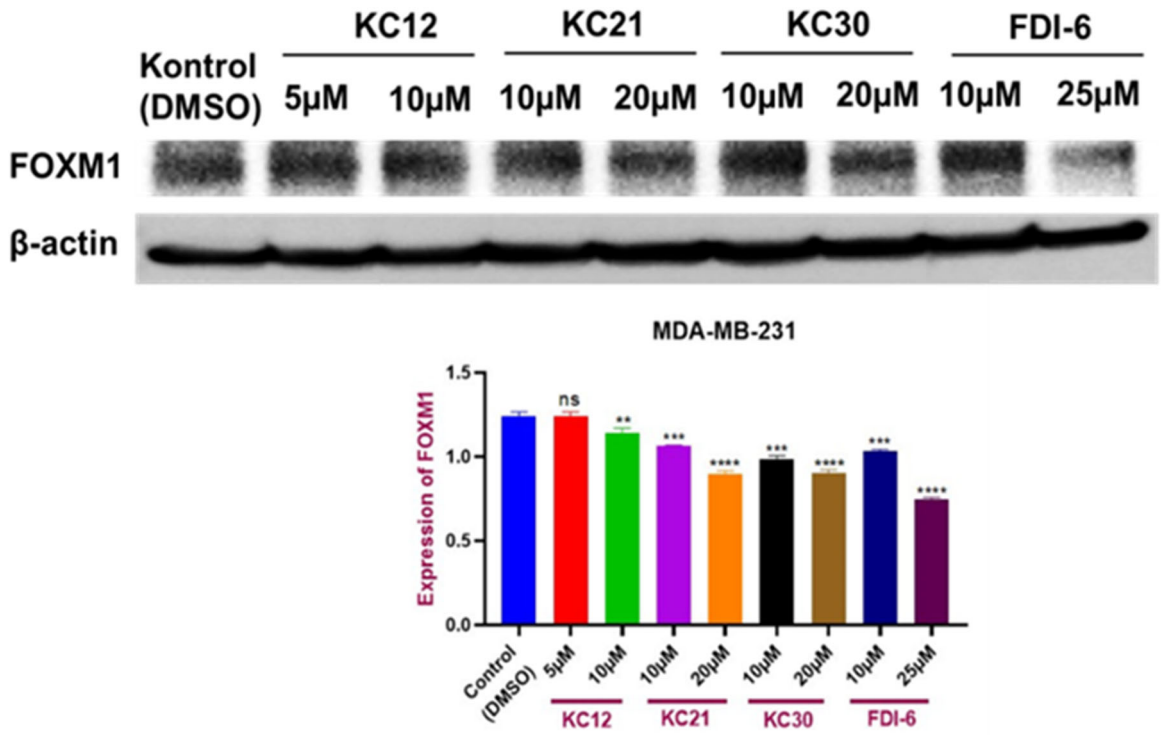


**FIGURE 14** Evaluation of dose-dependent FOXM1 protein expression levels by the selected compounds in MDA-MB-231 after 96 h of treatment. The compounds and the FDI-6 (25 μM) were used at indicated doses. Statistical significance was determined using one-way ANOVA, with significance levels indicated as follows: ** = $p \leq 0.01$, *** = $p \leq 0.001$, **** = $p \leq 0.0001$ compared to the DMSO control.

5-[4-(Dimethylamino)benzylidene]thiazolidine-2,4-dione (**KC27 (d)**): Method vi. Orange solid; yield, 89%; m.p.: 291-292 °C; lit. m.p.: 282–283°C.[48] FT-IR υ ($cm^{-1}$): 3097 (N-H), 2996–2952 (C-H), 2827 (C-H -$CH_3$), 2767 (N-H.....O intra-hydrogen bond), 1722, 1681 (C=O), 1612 (C=C), 1519–1437 (C=C), 1381 (C-H, -$CH_3$), 1329, 1234 (C-N), 1188, 1137 (O=C-N-C=O), 901 (C-S).

5-[(1*H*-Pyrrol-2-yl)methylene]thiazolidine-2,4-dione (**KC28 (d)**): Method vii. Dark yellow solid; yield, 41%; M.P. 256–258°C. FT-IR υ ($cm^{-1}$): 3321, 3117 (N-H), 3099 (C=C-H), 2962 (C-H), 2775 (N-H.....O intra-hydrogen bond), 1704, 1668 (C=O), 1574 (C=C), 1485–1423 (C=C), 1328 (C-N-C), 1285 (C-N), 1155, 1115 (O=C-N-C=O), and 881 (C-S).

5-(Furan-2-ylmethylene)thiazolidine-2,4-dione (**KC29 (d)**): Method vii. Brown solid; yield, 51%; M.P. 240–241°C; lit. M.P. 238°C.[80] FT-IR υ ($cm^{-1}$): 3129 (N-H), 3009 (C-H), 2787 (N-H.....O intra-hydrogen bond), 1720, 1677 (C=O), 1607 (C=C), 1543, 1516 (C=C), 1337 (C-O-C), 1284 (C-N), 1166, 1148 (O=C-N-C=O), and 884 (C-S).

5-(2-Hydroxy-5-methoxybenzylidene)thiazolidine-2,4-dione (**KC30 (d)**): Method vii. Dark yellow solid; yield, 51%; M.P. 210–212°C. FT-IR υ ($cm^{-1}$): 3427, 3156 (N-H), 3066–2952 (C-H), 2839 (C-H -$CH_3$), 2783 (N-H.....O intra-hydrogen bond), 1732, 1696 (C=O), 1588 (C=C), 1499-1443 (C=C), 1344 (C-H, -$CH_3$), 1326, 1259, 1034, 1021 (C-O), 1243 (C-N), 1192, 1149 (O=C-N-C=O), and 822 (C-S).

5-(2,5-Dimethoxybenzylidene)thiazolidine-2,4-dione (**KC31 (d)**): Method vi. Orange solid; yield, 83%; M.P. 225–227°C. FT-IR υ ($cm^{-1}$): 3171 (N-H), 3080 (C=C-H), 3005–2980 (C-H), 2947, 2844 (C-H), 1735, 1701 (C=O), 1603 (C=C), 1484–1433 (C=C), 1387 and 1385 (C-H, -$CH_3$), 1297, 1287, 1066, 1051 (O-C), 1287 (C-N), 1154, and 1066 (O=C-N-C=O).

5-(3,4,5-Trimethoxybenzylidene)thiazolidine-2,4-dione (**KC32 (d)**): Method vi. Light yellow solid; yield, 92%; M.P. 185–187°C; lit. M.P. 185–187°C,[81] 210°C.[79] FT IR υ ($cm^{-1}$): 3163 (N-H), 3054–2993 (C-H), 2943, 2835 (C-H $CH_3$), 2762 (N-H.....O intra-hydrogen bond), 1727, 1679 (C=O), 1603 (C=C), 1501-1452 (C=C), 1418 (C-H, -$CH_3$), 1308, 1292 (O-C), 1240 (C-N), 1145, 1120 (O=C-N-C=O), and 905 (C-S).

5-(4-Hydroxybenzylidene)thiazolidine-2,4-dione (**KC33 (d)**): Method vii. Yellow solid; yield, 46%; M.P. 282–284°C; lit. M.P. 309–310°C,[79] 283–285°C.[48] FT-IR υ ($cm^{-1}$): 3400 (O-H), 3122 (N-H), 2991–2960 (C-H), 2790 (N-H.....O intra-hydrogen bond), 1718, 1671 (C=O), 1570 (C=C), 1508–1477 (C=C), 1338, 1023 (C-O), 1278 (C-N), 1152, 1117 (O=C-N-C=O), and 899 (C-S).

5-[4-(Trifluoromethyl)benzylidene]thiazolidine-2,4-dione (**KC34 (d)**): Method vi. Cream solid, yield, 38%; M.P. 186–188°C. FT-IR υ ($cm^{-1}$): 3197 (N-H), 3052 (C-H), 2734 (N-H.....O intra-hydrogen bond), 1749, 1673 (C=O), 1606 (C=C), 1587, 1575 (C=C), 1313 (C-F), 1290 (C-N), 1154, 1119 (O=C-N-C=O), and 898 (C-S).

5-(4-Chlorobenzylidene)thiazolidine-2,4-dione (**KC35 (d)**): Light yellow solid; yield, 92%; M.P. 233–235°C; lit. M.P. 228°C.[79] FT-IR υ ($cm^{-1}$): 3178 (N-H), 3090 (C=C-H), 3056 (C-H), 2761 (N-H.....O intra-hydrogen bond), 1756, 1691 (C=O), 1610 (C=C), 1575, 1484 (C=C), 1278 (C-N), 1153, 1091 (O=C-N-C=O), and 897 (C-S).

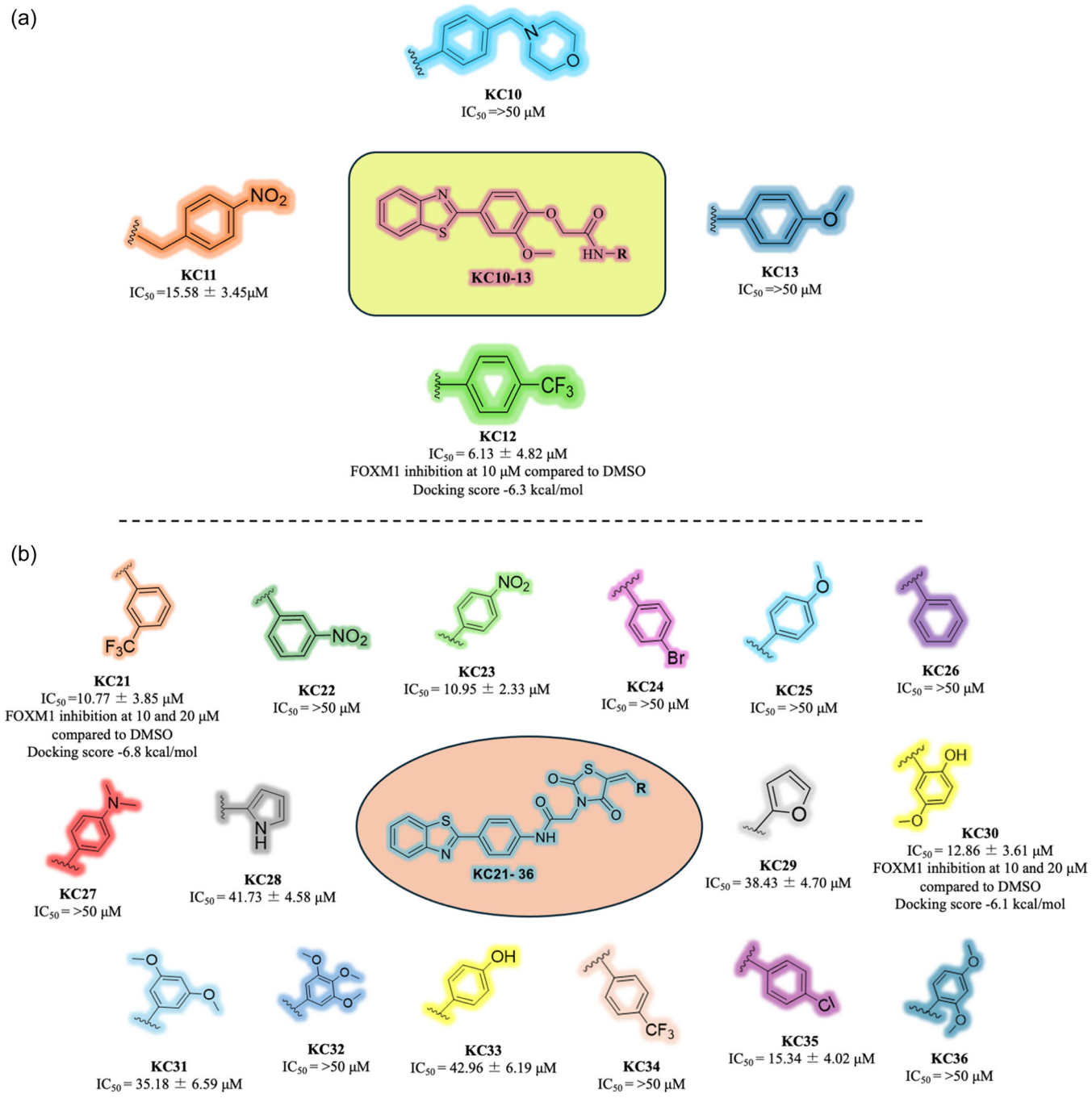


**FIGURE 15** Structure–Activity Relationship (SAR) study of the synthesized compounds.

5-(2,4-Dimethoxybenzylidene)thiazolidine-2,4-dione (**KC36 (d)**): Method vii. Yellow solid; yield, 49%; M.P. 258–259°C. lit. M.P. 250°C,[82] 240–242°C.[83] FT-IR υ ($cm^{-1}$): 3102 (N-H), 2991–2948 (C-H), 2948, 2842 (C-H, -$CH_3$), 2781 (N-H.....O intra-hydrogen bond), 1718, 1683 (C=O), 1567 (C=C), 1575–1452 (C=C), 1353 (C-H, -$CH_3$), 1314, 1020 (O-C), 1264 (C-N), 1161, 1117 (O=C-N-C=O), and 824 (C-S).

*Synthesis of the benzothiazole-thiazolidine-2,4-dione derivatives* ***KC21–KC36***

A mixture of *N*-[4-(benzo[d]thiazol-2-yl)phenyl]-2-bromoacetamide **(8)** (1 mmol), Knoevenagel compounds (**KC21–KC36 (d)**) (1 mmol), and anhydrous $K_2CO_3$ (0.02 g; 0.15 mmol) was stirred in 5 mL DMF at 70°C for 12–24 h. Subsequently, the reaction mixture was cooled, poured into cold water, and stirred at room temperature for an additional 30 min. The resulting precipitate was filtered, washed with water, and dried. The reaction progress was assessed by TLC using a mixture toluene: ethyl acetate: formic acid TEF (4:3:1) as a mobile phase. The crude product underwent recrystallization from a mixture of EtOH:DMF (7:3). Compound purity was further confirmed using TLC and TEF. The impure compounds were further purified through a silica column using the solvent mixture of *n*-hexane/ethyl acetate (1:2).

*N*-[4-(Benzo[d]thiazol-2-yl)phenyl]-2-{5-[3-(trifluoromethyl) benzylidene]-2,4-dioxothiazolidin-3-yl}acetamide (**KC21**): Cream solid; yield, 60%; M.P. 268–270°C. FT-IR υ ($cm^{-1}$): 3185 (N-H), 3113 (H-C=C), 3024 (C-H), 2990, 2956 (C-H), 1714, 1676, and 1668 (C=O), 1605 (N-H), 1533 (C=N), 1533 (C=C), 1507–1483 (C=C), 1433 (C-H, -$CH_2$), 1332 (C-F), 1284 (C-N), 1121, 1086 (O=C-N-C=O), 901 (C-S-C); $^1$H-NMR (400 MHz, DMSO-$d_6$): δ 10.75 (s, 1H), 8.14–8.08 (m, 2H), 8.08–8.02 (m, 3H), 7.99 (dd, *J* = 8.1, 2.5 Hz, 1H), 7.91 (d, *J* = 7.6 Hz, 1H), 7.85 (d, *J* = 8.0 Hz, 1H), 7.79 (dd, *J* = 8.0, 2.5 Hz, 1H), 7.74 (dd, *J* = 8.8, 2.9 Hz, 2H), 7.50 (td, *J* = 8.0, 2.0 Hz, 1H), 7.41 (td, *J* = 7.6, 2.4 Hz, 1H), 4.57 (s, 2H); $^{13}$C-NMR (100 MHz, DMSO-$d_6$): δ 166.86, 166.78, 165.11, 164.29, 153.65, 141.18, 134.36, 134.04, 132.85, 132.14, 130.66, 130.95 (q, $^2J_{CF}$ = 32.9 Hz), 128.23, 128.12, 127.42, 127.01, 126.98 (q, $^1J_{CF}$ = 272.6 Hz), 126.67, 125.38, 123.17, 122.69, 122.36, 119.51, 44.34; LC-MS (*m/z*): 540 ($[M + H]^+$ 100.00%).

*N*-[4-(Benzo[d]thiazol-2-yl)phenyl]-2-[5-(4-nitrobenzylidene)-2,4-dioxothiazolidin-3-yl]acetamide (**KC22**): Yellow crystal; yield, 93%, M.P. 254–255°C. FT-IR υ ($cm^{-1}$): 3358 (N-H), 3111 (H-C=C), 3075–3032, (C-H), 2936 (C-H), 1736, 1684, and 1675 (C=O), 1617 (N-H), 1587 (C=N), 1515, 1328 ($NO_2$), 1477 (C=C), 1435 (C-H, -$CH_2$), 1341, 1304, 1087 (C-N), 1193, 1145 (O=C-N-C=O), 967 (C-S-C). $^1$H-NMR (500 MHz, DMSO-$d_6$): δ 10.83 (s, 1H), 8.32 (d, *J* = 8.7 Hz, 2H), 8.07 (d, *J* = 7.6 Hz, 2H), 8.02 (d, *J* = 8.7 Hz, 2H), 7.97 (d, *J* = 8.1 Hz, 1H), 7.89 (d, *J* = 8.7 Hz, 2H), 7.73 (d, *J* = 8.4 Hz, 2H), 7.48 (t, *J* = 7.7 Hz, 1H), 7.39 (t, *J* = 7.6 Hz, 1H), 4.56 (s, 2H). $^{13}$C-NMR (150 MHz, DMSO-$d_6$): δ 167.92, 167.33, 165.98, 154.07, 152.24, 141.66, 135.16, 134.78, 132.98, 128.63, 128.50, 127.11, 125.82, 123.09, 122.77, 120.07, 119.94, 113.21, 112.59, 44.44; LC-MS (*m/z*): 515.050 ($[M - 1]^+$ 100.00%).

*N*-[4-(Benzo[d]thiazol-2-yl)phenyl]-2-[5-(3-nitrobenzylidene)-2,4-dioxothiazolidin-3-yl]acetamide (**KC23**): Yellow solid; yield, 49%; M.P. 291–293°C. FT-IR υ ($cm^{-1}$): 3251 (N-H), 3110 (H-C=C), 3062, 2993 (C-H), 2951 (C-H), 1750, 1694, and 1666 (C=O), 1573 (C=C), 1604 (C=N), 1533, 1351 (N=O), 1484 (C=C), 1435 (C-H, -$CH_2$), 1255 (C-N), 1152, 1104 (O=C-N-C=O), 921 (C-S-C). $^1$H-NMR (400 MHz, DMSO-$d_6$): δ 10.75 (s, 1H), 8.51 (s, 1H), 8.30 (d, *J* = 8.2 Hz, 1H), 8.17 (s, 1H), 8.10 (d, *J* = 7.1 Hz, 1H), 8.06 (d, *J* = 8.9 Hz, 3H), 8.00 (d, *J* = 8.0 Hz, 1H), 7.83 (t, *J* = 8.0 Hz, 1H), 7.74 (d, *J* = 8.7 Hz, 2H), 7.50 (t, *J* = 7.8 Hz, 1H), 7.41 (t, *J* = 7.3 Hz, 1H), 4.58 (s, 2H). $^{13}$C-NMR (100 MHz, DMSO-$d_6$): δ 167.35, 167.09, 165.51, 164.73, 154.14, 148.85, 141.65, 135.98, 135.05, 134.86, 132.02, 131.55, 128.86, 128.71, 127.16, 125.87, 126.05–125.10 (m), 124.43, 123.16, 122.83, 120.04, 44.86. LC-MS (*m/z*): 516 ($[M + H]^+$ 28%) and 515 ($[M - 1]^+$ 100.00%).

*N*-[4-(Benzo[d]thiazol-2-yl)phenyl]-2-[5-(4-bromobenzylidene)-2,4-dioxothiazolidin-3-yl]acetamide (**KC24**): White solid; yield, 75%, M.P. 249–251°C. FT-IR υ ($cm^{-1}$): 3349 (N-H), 3059 (C-H), 2976, 2936 (C-H), 1736, 1684, and 1672 (C=O), 1548 (C=C), 1612 (N-H), 1591 (C=N), 1521–1520, 1480 (C=C), 1434 (C-H, -$CH_2$), 1242 (C-N), 1196, 1145 (O=C-N-C=O), 893 (C-S-C). $^1$H-NMR (400 MHz, DMSO-$d_6$): δ 10.73 (s, 1H), 8.09 (d, *J* = 8.0 Hz, 1H), 8.04 (d, *J* = 8.8 Hz, 2H), 7.98 (d, *J* = 8.1 Hz, 1H), 7.96 (s, 1H), 7.74 (d, *J* = 6.1 Hz, 3H), 7.72 (d, *J* = 6.4 Hz, 3H), 7.59 (d, *J* = 8.4 Hz, 2H), 7.49 (t, *J* = 7.6 Hz, 1H), 7.40 (t, *J* = 7.2 Hz, 1H), 4.54 (s, 2H). $^{13}$C-NMR (100 MHz, DMSO-$d_6$): δ 167.42, 167.35, 165.73, 164.81, 154.13, 141.66, 134.83, 133.06, 132.99, 132.60, 132.56, 128.71, 128.59, 127.16, 125.87, 124.97, 123.16, 122.86, 122.27, 119.99, 44.76. LC-MS (*m/z*): 550 ($[M + H]^+$ 98.92%) and 552 ($[M + 2]^+$ 100.00%).

*N*-[4-(Benzo[d]thiazol-2-yl)phenyl]-2-[5-(4-methoxybenzylidene)-2,4 dioxothiazolidin-3-yl]acetamide (**KC25**): Light yellow solid; yield, 78%; M.P. 305–307°C. FT-IR υ ($cm^{-1}$): 3266 (N-H), 3119 (H-C=C), 3052–3012, (C-H), 2929 (C-H), 2834 ($OCH_3$), 1742, 1686, and 1667 (C=O), 1634 (N-H), 1590 (C=N), 1540 (C=C), 1511, 1485 (Ar C=C), 1435 (C-H, -$CH_2$), 1407 (C-H, -$CH_3$), 1379, 1308, 1098 (C-N), 1261, 1032 (C-O-C), 1151, 1117 (O=C-N-C=O), 967 (C-S-C). $^1$H-NMR (400 MHz, DMSO-$d_6$): δ 10.73 (s, 1H), 8.09 (d, *J* = 8.0 Hz, 1H), 8.04 (d, *J* = 8.8 Hz, 2H), 7.98 (d, *J* = 8.1 Hz, 1H), 7.96 (s, 1H), 7.74 (d, *J* = 6.1 Hz, 3H), 7.72 (d, *J* = 6.4 Hz, 3H), 7.59 (d, *J* = 8.4 Hz, 2H), 7.49 (t, *J* = 7.6 Hz, 1H), 7.40 (t, *J* = 7.2 Hz, 1H), 4.54 (s, 2H). $^{13}$C-NMR (100 MHz, DMSO-$d_6$): δ 167.69, 167.30, 165.88, 164.86, 161.82, 154.09, 141.64, 134.79, 134.18, 132.89, 128.63, 128.53, 127.09, 125.80, 123.10, 122.77, 119.95, 118.08, 115.53, 56.03, 44.59. LC-MS (*m/z*): 502.100 ($[M + H]^+$ 100.00%).

*N*-[4-(Benzo[d]thiazol-2-yl)phenyl]-2-(5-benzylidene-2,4-dioxothiazolidin-3-yl)acetamide (**KC26**): White solid; yield, 29%; M.P. 302–304°C. FT-IR υ ($cm^{-1}$): 3264 (N-H), 3114 (H-C=C), 3048-3026 (C-H), 2945 (C-H), 1748, 1687, and 1665 (C=O), 1598 (C=N), 1540 (C=C), 1536, 1480 (C=C), 1447 (C-H, -$CH_2$), 1251 (C-N), 1149, 1109 (O=C-N-C=O), 920 (C-S-C). $^1$H-NMR (400 MHz, DMSO-$d_6$): δ 10.74 (s, 1H), 8.10 (d, *J* = 8.2 Hz, 1H), 8.05 (d, *J* = 8.2 Hz, 2H), 8.00 (d, 1H), 7.99 (s, 1H), 7.74 (d, *J* = 8.5 Hz, 2H), 7.65 (d, *J* = 7.4 Hz, 2H), 7.58–7.52 (m, 3H), 7.50 (t, *J* = 7.3 Hz, 1H), 7.41 (t, *J* = 7.6 Hz, 1H), 4.56 (s, 2H). $^{13}$C-NMR (100 MHz, DMSO-$d_6$): δ 166.53, 166.22, 164.69, 163.71, 153.01, 140.54, 133.71, 133.12, 132.25, 130.26, 129.63, 129.18, 128.85, 128.59, 127.56, 127.48, 126.01, 124.73, 122.03, 121.70, 120.34, 118.88, 43.59. LC-MS (*m/z*): 472 ($[M + H]^+$ 64.56%).

*N*-[4-(Benzo[d]thiazol-2-yl)phenyl]-2-{5-[4-(dimethylamino) benzylidene]-2,4-dioxothiazolidin-3-yl}acetamide (**KC27**): Yellow solid; yield, 68%; M.P. 236–237°C. FT-IR υ ($cm^{-1}$): 3356 (N-H), 3115 (H-C=C), 3062–2988 (C-H), 2940 (C-H), 2861–2805 (N($CH_3$)$_2$ C-H), 1731, 1698, and 1668 (C=O), 1571 (C=N), 1524 (C=C), 1482 (Ar C=C), 1433 (C-H, -$CH_2$), 1404 (C-H, -$CH_3$), 1364, 1306, 1086 (C-N), 1198, 1138 (O=C-N-C=O), 967 (C-S-C). $^1$H-NMR (500 MHz, DMSO-$d_6$): δ 10.67 (s, 1H), 8.07 (d, *J* = 8.0 Hz, 1H), 8.02 (d, *J* = 8.5 Hz, 2H), 7.97 (d, *J* = 8.1 Hz, 1H), 7.80 (s, 1H), 7.71 (d, *J* = 8.5 Hz, 2H), 7.50–7.42 (m, 3H), 7.38 (t, *J* = 7.6 Hz, 1H), 6.79 (d, *J* = 8.7 Hz, 2H), 4.49 (s, 2H), 2.98 (s, 6H). $^{13}$C-NMR (150 MHz, DMSO-$d_6$): δ 167.93, 167.33, 165.98, 165.02, 154.07, 152.24, 141.66, 135.16, 134.78, 132.99, 128.63, 128.50, 127.11, 125.82, 123.10, 122.77, 120.07, 119.94, 113.21, 112.59, 44.44. LC-MS (*m/z*): 515.100 ($[M + H]^+$ 100.00%).

2-{5-[(1*H*-Pyrrol-2-yl)methylene]-2,4-dioxothiazolidin-3-yl}-N-[4-(benzo[d]thiazol-2-yl)phenyl]acetamide (**KC28**): Light green solid; yield, 76%; M.P. 337–339°C. FT-IR υ ($cm^{-1}$): 3335 (N-H, pyrrole),

3269 (N-H), 3121 (H-C=C), 3057, 2999 (C-H), 2951 (C-H), 1734, 1671, and 1657 (C=O), 1599 (C=N), 1536 (C=C), 1482 (C=C), 1434 (C-H, -$CH_2$), 1372, 1307, 1053 (C-N), 1139, 1115 (O=C-N-C=O), 969 (C-S-C). $^1$H-NMR (400 MHz, DMSO-$d_6$): δ 11.76 (s, 1H), 10.70 (s, 1H), 8.10 (d, *J* = 7.9 Hz, 1H), 8.08–8.02 (m, 2H), 8.00 (d, *J* = 8.1 Hz, 1H), 7.86–7.79 (m, 1H), 7.78–7.71 (m, 2H), 7.51 (t, *J* = 7.6 Hz, 1H), 7.42 (t, *J* = 7.4 Hz, 1H), 7.24 (s, 1H), 6.61–6.52 (m, 1H), 6.51–6.33 (m, 1H), 4.51 (s, 2H). $^{13}$C-NMR (100 MHz, DMSO-$d_6$): δ 167.79, 167.30, 165.96, 164.90, 160.82, 154.09, 141.65, 134.79, 134.61, 133.23, 128.63, 128.52, 127.09, 125.80, 124.24, 123.10, 122.78, 119.94, 116.94, 116.74, 44.55. LC-MS (*m/z*): 461.100 ([M + H]$^+$ 100.00%).

*N*-[4-(Benzo[d]thiazol-2-yl)phenyl]-2-[5-(furan-2-ylmethylene)-2,4-dioxothiazolidin-3-yl]acetamide (**KC29**): Brown solid; yield, 46%; M.P. 301–303°C. FT-IR υ (cm$^{-1}$): 3260 (N-H), 3127 (H-C=C), 3044 (C-H), 2943 (C-H), 1742, 1684, and 1668 (C=O), 1616 (N-H), 1604 (C=N), 1537 (C=C), 1482 (C=C), 1435 (C-H, -$CH_2$), 1408, 1383 (O-C), 1253 (C-N), 1151, 1112 (O=C-N-C=O), 885 (C-S-C). $^1$H-NMR (400 MHz, DMSO-$d_6$): δ 10.68 (s, *J* = 5.6 Hz, 1H), 8.08 (d, *J* = 6.7 Hz, 2H), 8.03 (d, *J* = 8.5 Hz, 2H), 7.98 (d, *J* = 7.9 Hz, 1H), 7.79 (s, 1H), 7.72 (d, *J* = 8.5 Hz, 2H), 7.48 (t, *J* = 7.7 Hz, 1H), 7.39 (t, *J* = 7.3 Hz, 2H), 7.15 (d, *J* = 3.7 Hz, 1H), 6.77–6.72 (m, 1H), 4.51 (s, 2H). $^{13}$C-NMR (125 MHz, DMSO-$d_6$): δ 173.08, 172.05, 170.31, 169.61, 158.85, 154.39, 154.39, 146.39, 139.54, 133.39, 133.28, 131.84, 130.55, 127.86, 127.52, 125.31, 124.95, 124.69, 122.69, 118.95, 49.26. LC-MS (*m/z*): 462 ([M + H]$^+$ 100.00%).

*N*-[4-(Benzo[d]thiazol-2-yl)phenyl]-2-[5-(2-hydroxy-5-methoxybenzylidene)-2,4-dioxothiazolidin-3-yl]acetamide (**KC30**): Brown solid; yield, 15%; M.P. 262–263°C. FT-IR υ (cm$^{-1}$): 3334 (O-H), 3291 (N-H), 3106 (H-C=C), 3055–3004, (C-H), 2953 (C-H), 2834 ($OCH_3$), 1731, 1682, and 1667 (C=O), 1593 (C=N), 1540 (C=C), 1511, 1481 (C=C), 1434 (C-H, -$CH_2$), 1406 (C-H, -$CH_3$), 1380, 1285, 1087 (C-N), 1254, 1206, 1039, 1019 (C-O-C), 1151, 1119 (O=C-N-C=O), 964 (C-S-C). $^1$H-NMR (500 MHz, DMSO-$d_6$): δ 10.84 (s, 1H), 10.29 (s, 1H), 8.20 (d, *J* = 8.0 Hz, 2H), 8.15 (d, *J* = 8.4 Hz, 2H), 8.10 (d, *J* = 8.2 Hz, 1H), 7.84 (d, *J* = 8.4 Hz, 2H), 7.61 (t, *J* = 7.7 Hz, 1H), 7.52 (t, *J* = 7.6 Hz, 1H), 7.07 (dd, *J* = 9.0, 2.7 Hz, 1H), 7.01 (d, *J* = 8.9 Hz, 1H), 6.96 (td, *J* = 2.1 Hz, 1H), 4.64 (s, 2H), 3.82 (s, 3H). $^{13}$C-NMR (125 MHz, DMSO-$d_6$, ppm): δ 167.81, 167.32, 165.93, 164.86, 154.08, 152.71, 152.07, 141.64, 134.79, 129.58, 128.64, 127.10, 125.82, 123.11, 122.78, 120.33, 120.22, 119.96, 119.84, 117.75, 112.62, 55.98, 44.57. LC-MS (*m/z*): ([M + H]$^+$ 100.00%).

*N*-[4-(Benzo[d]thiazol-2-yl)phenyl]-2-[5-(3,5-dimethoxybenzylidene)-2,4-dioxothiazolidin-3-yl]acetamide (**KC31**): White solid; yield, 62%; M.P. 259–260°C. FT-IR υ (cm$^{-1}$): 3270 (N-H), 3081 (H-C=C), 3044 (C-H), 2943 (C-H), 1740 and 1667 (C=O), 1605 (N-H), 1590 (C=N), 1541 (C=C), 1536–1408 (C=C), 1455 (C-H, -$CH_2$), 1330, 1299, 1070, and 1054 (O-C), 1255 (C-N), 1157, 1196 (O=C-N-C=O), 912 (C-S-C). $^1$H-NMR (400 MHz, DMSO-$d_6$): δ 10.79 (s, 1H), 8.10 (d, *J* = 7.5 Hz, 1H), 8.05 (d, *J* = 8.7 Hz, 2H), 7.99 (d, *J* = 8.2 Hz, 1H), 7.91 (s, 1H), 7.74 (d, *J* = 8.7 Hz, 2H), 7.50 (t, *J* = 7.6 Hz, 1H), 7.41 (t, *J* = 7.6 Hz, 1H), 6.79 (d, *J* = 2.3 Hz, 2H), 6.64 (dd, *J* = 2.7, 2.0 Hz, 1H), 4.55 (s, 2H), 3.77 (s, 6H). $^{13}$C-NMR (100 MHz, DMSO-$d_6$): δ 167.57, 167.36, 165.73, 164.85, 161.44, 154.15, 141.68, 135.24, 134.85, 134.27, 128.71, 128.61, 127.16, 125.88, 123.17, 122.85, 122.14, 120.00, 108.47, 103.30, 56.03, 44.72. LC-MS (*m/z*): 532 ([M + H]$^+$ 14.78%).

*N*-[4-(Benzo[d]thiazol-2-yl)phenyl]-2-[2,4-dioxo-5-(3,4,5 trimethoxybenzylidene)thiazolidin-3-yl]acetamide (**KC32**): Light yellow solid; yield, 75%; M.P. 266–267°C. FT-IR υ (cm$^{-1}$): 3374 (N-H), 3108 (H-C=C), 3046–3007, (C-H), 2926 (C-H), 2854, 2836 ($OCH_3$), 1737, 1703, and 1675 (C=O), 1589 (C=N), 1537 (C=C), 1509, 1480 (C=C), 1433 (C-H, -$CH_2$), 1406 (C-H, -$CH_3$), 1381, 1294, 1085 (C-N), 1273, 1255, 1031, 1014 (C-O), 1159, 1132 (O=C-N-C=O), 970 (C-S-C). $^1$H-NMR (500 MHz, DMSO-$d_6$): δ 10.82 (s, 1H), 8.20 (d, *J* = 7.9 Hz, 1H), 8.15 (d, *J* = 8.3 Hz, 2H), 8.09 (d, *J* = 8.1 Hz, 1H), 8.03 (s, 1H), 7.84 (d, *J* = 8.3 Hz, 2H), 7.60 (t, *J* = 7.6 Hz, 1H), 7.51 (t, *J* = 7.5 Hz, 1H), 7.07 (s, 2H), 4.65 (s, 2H), 3.92 (s, 6H), 3.81 (s, 3H). $^{13}$C-NMR (125 MHz, DMSO-$d_6$): δ 167.59, 167.30, 165.73, 164.81, 154.10, 153.75, 141.63, 140.22, 134.79, 134.42, 128.83, 128.65, 128.55, 127.10, 125.82, 123.11, 122.78, 120.36, 119.96, 108.24, 60.72, 56.55, 44.63. LC-MS (*m/z*): 560.100 ([M + H]$^+$ 100.00%).

*N*-[4-(Benzo[d]thiazol-2-yl)phenyl]-2-[5-(4-hydroxybenzylidene)-2,4-dioxothiazolidin-3-yl]acetamide (**KC33**): Yellow solid; yield, 20%; m.p.: 315-317 °C. FT-IR υ (cm$^{-1}$): 3320 (O-H), 3287 (N-H), 3114 (H-C = C), 3059, 3032 (C-H), 2942 (C-H), 1738 and 1669 (C = O), 1587 (C = N), 1536 (C = C), 1510, 1478 (C = C), 1435 (C-H, -$CH_2$), 1376, 1311, 1088 (C-N), 1284, 1088 (O-C), 1174, 1144 (O = C-N-C = O), 967 (C-S-C). $^1$H-NMR (400 MHz, DMSO-$d_6$): δ 10.71 (s, 1H), 10.39 (s, 1H), 8.10 (d, *J* = 8.0 Hz, 1H), 8.05 (d, *J* = 8.7 Hz, 2H), 8.00 (d, *J* = 8.1 Hz, 1H), 7.88 (s, 1H), 7.74 (d, *J* = 8.5 Hz, 2H), 7.54 – 7.47 (m, 3H), 7.41 (t, *J* = 7.6 Hz, 1H), 6.92 (d, *J* = 8.4 Hz, 2H), 4.53 (s, 2H). $^{13}$C-NMR (125 MHz, DMSO-$d_6$): δ 167.81, 167.31, 165.96, 164.91, 160.81, 154.08, 141.64, 134.78, 134.62, 133.24, 128.64, 128.53, 127.10, 125.81, 124.24, 123.10, 122.78, 119.95, 116.94, 116.75, 44.54. LC-MS(m/z): 488.050 ([M + H]$^+$ 100.00%).

*N*-[4-(Benzo[d]thiazol-2-yl)phenyl]-2-{2,4-dioxo-5-[4-(trifluoromethyl)benzylidene]thiazolidin-3-yl}acetamide (**KC34**): White solid; yield, 89%; M.P. 286–288°C. FT-IR υ (cm$^{-1}$): 3355 (N-H), 3107 (H-C=C), 3059–2976 (C-H), 2937 (C-H), 1738, 1686, and 1675 (C=O), 1619 (N-H), 1591 (C=N), 1520 (C=C), 1482–1408 (Ar C=C), 1435 (C-H, -$CH_2$), 1320 (C-F), 1305 (C-N), 1167, 1117 (O=C-N-C=O), 895 (C-S-C). $^1$H-NMR (500 MHz, DMSO-$d_6$): δ 10.76 (s, 1H), 8.13 (dd, *J* = 8.2, 1.3 Hz, 1H), 8.09 (dd, *J* = 8.4, 1.7 Hz, 2H), 8.03 (dd, *J* = 7.6, 1.4 Hz, 1H), 7.93 (d, *J* = 8.6 Hz, 2H), 7.90 (d, *J* = 8.4 Hz, 2H), 7.78 (dd, *J* = 9.0, 1.7 Hz, 2H), 7.54 (td, *J* = 8.3, 1.4 Hz, 1H), 7.45 (td, *J* = 8.3, 1.2 Hz, 1H), 4.61 (s, 2H). $^{13}$C-NMR (125 MHz, DMSO-$d_6$): 166.20, 166.18, 164.46, 163.62, 153.01, 140.51, 136.24, 133.71, 131.31, 130.11, 129.56 (q, $^2J_{CF}$ = 33.6 Hz), 127.57, 127.50, 126.02, 125.60 (q, $^3J_{CF}$ = 3.9 Hz), 124.73, 123.34, 123.23 (q, $^1J_{CF}$ = 273.7 Hz), 122.03, 121.70, 118.89, 43.70. LC-MS (*m/z*): 539 ([M + H]$^+$ 13.23%), 540 ([M – 1]$^+$ 100.00%).

*N*-[4-(Benzo[d]thiazol-2-yl)phenyl]-2-[5-(4-chlorobenzylidene)-2,4-dioxothiazolidin-3-yl]acetamide (**KC35**): Light yellow solid; yield, 71%; M.P. 341–342°C. FT-IR υ (cm$^{-1}$): 3346 (N-H), 3061 (H-C=C), 3007, 2977 (C-H), 2937 (C-H), 1738, 1688, and 1673 (C=O), 1611

(N-H), 1596 (C=N), 1522 (C=C), 1481, 1408 (C=C), 1435 (C-H, -$CH_2$), 1250 (C-N), 1145, 1085 (O=C-N-C=O), 895 (C-S-C). $^1$H-NMR (400 MHz, DMSO-$d_6$): δ 10.72 (s, 1H), 8.09 (d, *J* = 7.1 Hz, 1H), 8.08–8.01 (m, 2H), 7.99 (d, *J* = 6.9 Hz, 1H), 7.73 (d, *J* = 8.6 Hz, 2H), 7.67 (d, *J* = 8.2 Hz, 2H), 7.63–7.37 (m, 5H), 4.56 (s, 2H). $^{13}$C-NMR (100 MHz, DMSO-$d_6$): δ 167.41, 167.35, 165.72, 164.80, 154.15, 141.66, 135.99, 134.85, 132.95, 132.40, 132.30, 130.05, 128.70, 128.63, 127.15, 125.86, 123.17, 122.83, 122.23, 120.03, 44.76. LC-MS (*m/z*): 506 ([M + H]$^+$ 100.00%), 540 ([M + 2]$^+$ 52.51%).

*N*-[4-(Benzo[d]thiazol-2-yl)phenyl]-2-[5-(2,4-dimethoxybenzylidene)-2,4-dioxothiazolidin-3-yl]acetamide (**KC36**): Light yellow solid; yield, 28%; M.P. 287–289°C. FT-IR υ (cm$^{-1}$): 3375 (N-H), 3108 (H-C=C), 3068–3008 (C-H), 2939 (C-H), 2859, 2835 (O$CH_3$), 1738, 1705, and 1677 (C=O), 1590 (C=N), 1538 (C=C), 1507, 1481 (C=C), 1434 (C-H, -$CH_2$), 1407 (C-H, -$CH_3$), 1383, 1331, 1087 (C-N), 1295, 1274, 1087, 1032 (O-C), 1160, 1133 (O=C-N-C=O), 971 (C-S-C). $^1$H-NMR (500 MHz, DMSO-$d_6$): δ 10.80 (s, 1H), 8.20 (d, *J* = 8.0 Hz, 1H), 8.15 (d, *J* = 8.4 Hz, 3H), 8.09 (d, *J* = 8.1 Hz, 1H), 7.83 (d, *J* = 8.4 Hz, 2H), 7.60 (t, *J* = 7.7 Hz, 1H), 7.54–7.48 (m, 2H), 6.84–6.76 (m, 2H), 4.62 (s, 2H), 3.98 (s, 3H), 3.93 (s, 3H). $^{13}$C-NMR (125 MHz, DMSO-$d_6$): δ 168.00, 167.31, 166.07, 164.91, 163.99, 160.45, 154.10, 141.65, 134.79, 131.18, 129.05, 128.64, 128,53, 127.10, 125.81, 123.11, 122.78, 119.95, 117.86, 114.57, 107.22, 99.21, 56.47, 56.21, 44.52. LC-MS (*m/z*): 530.100 ([M + H]$^+$ 100.00%).

## 4.2 | Computational studies

### 4.2.1 | In silico studies for determining of physicochemical properties of new compounds

The physicochemical properties of synthesized compounds **KC10–KC13** and **KC21–KC36** were determined using the QikProp module within the Schrödinger software suite. Initially, the compounds were represented in 2D using ChemDraw and subsequently processed through the LigPrep module of Schrödinger's software following established protocols. The resulting structures were then input into the QikProp module to predict various pharmaceutically relevant properties. QikProp facilitated the determination of properties such as log water/gas, log octanol/water, log S, log $IC_{50}$ for HERG K+ channel blockage, Caco-2 value, log BB, log Khsa for human serum albumin binding, qualitative human oral absorption, human oral absorption on a scale of 0%–100%, and the number of violations of Lipinski's rule of 5.[51–53,84]

### 4.2.2 | Molecular docking

The crystal structure of the FOXM1 protein (PDB ID: 3G73) was obtained from the Protein Data Bank.[20,24,56] Before the docking experiments, preprocessing steps were applied to optimize the protein structures. Hetero atoms, water molecules, and chain A, C, and D were initially removed. Subsequently, only polar hydrogen atoms were added to the remaining protein structures. The resulting protein structures were then saved in.pdbqt format, ensuring compatibility for subsequent docking.[20]

Grid preparation was carried out using AutoDock Tools version 1.5.7 protocols. A comprehensive review of literature pertaining to the FOXM1-DBD was conducted to identify critical binding site residues related to the activity of FOXM1 for binding to DNA. Specific residues essential for FOXM1 and DNA interaction, including Asn283, Arg286, and His287, were identified.[20,24,54,56] The grid box for ligand binding to the FOXM1 DBD amino acid binding site was then determined.

The ligand preparation for the synthesized compounds began with their depiction in 2D using ChemDraw and subsequent saving in.sdf format to facilitate their readiness for molecular docking studies. Using Open Babel software (version 2.3.2),[85] the conversion of compounds from.sdf to.pdb files was performed. Subsequently, the ligand structures were prepared in AutoDock Tools (ADT) from MGL software packages (version 1.5.6). This involved assigning Gasteiger partial charges, and the structures were saved in a rigid format.[20,86,87] Following this, all structures underwent a transformation into.pdbqt format, making them suitable for use in subsequent investigations. Molecular docking was performed by using AutoDock Vina.[20,87] Subsequent analysis of the docking results, encompassing both 2D and 3D representations of ligand–receptor interactions, was conducted using the DS package (2021).

### 4.2.3 | MD simulation

The dynamic features of the protein–ligand complex were investigated through MD simulations using the Desmond software within the Schrodinger Maestro. Protein preparation wizard was used to prepare FOXM1 protein.[20,88,89] To mimic physiological conditions, the complex was immersed in a solvated environment consisting of an orthorhombic periodic box filled with simple point charge water. Neutralization was obtained by adding 150 mM NaCl solution. The solvated structure was then subjected to energy minimization and restrained to its initial location using the OPLS2005 force field.[90] Subsequently, 100 ns MD simulations were carried out under NPT ensemble at a temperature of 300K and a pressure of 1 atm.[20,89] The expected protein–ligand interactions were obtained during simulations and provided insights into the behavior and dynamics of the protein–ligand complex in the simulated environment.

## 4.3 | In vitro activity studies

### 4.3.1 | Cell lines and culture conditions

The antiproliferative activity of the synthesized compounds, including **KC10–KC13** and **KC21–KC36** was assessed using human TNBC cell line (MDA-MB 231, the American Type Culture Collection). The cells were cultivated in Dulbecco's Modified Eagle's Medium (DMEM)/F12,

supplemented with 10% fetal bovine serum (FBS; Sigma-Aldrich). Standard culture conditions of 37°C and 5% $CO_2$ were maintained in DMEM/F12 (1:1), supplemented with 10% FBS and 1% penicillin/streptomycin (PS).[16,19,20]

### 4.3.2 | Cell cytotoxicity assay (MTT assay)

For the assessment of cell cytotoxicity, the compounds were dissolved in DMSO and subsequently applied to the cells at concentrations ranging from 5 to 100 µM for a duration of 96 h. Untreated cells and those treated solely with DMSO served as controls. Following the designated time intervals, MTT solution (3-(4,5-dimethylthiazol-2-yl)-2,5-diphenyltetrazolium bromide) was introduced to each well, and the cells were incubated for 3 h at 37°C in a $CO_2$ incubator. Plate measurements were conducted at 570 nm using a Thermo Spectrophotometer. The acquired data were processed using GraphPad Prism 7 software. The cell viability percentages were calculated.[19,20,91]

### 4.3.3 | Western blot analysis

Western blot analysis was performed according to the methodology described in our previous studies.[16,17,20] MDA-MB-231 cells were treated with varying concentrations of the potent compounds **KC12, KC21**, and **KC30** (10 and 20 µM), as well as the positive control FDI-6 (10 and 25 µM), for a duration of 96 h. After the treatment period, cells were collected and washed with PBS. Lysis buffer containing phosphatase, protease, and NaCl (1%) was employed to extract lysates. Protein concentrations were determined using a BCA assay kit. The proteins, posttransfection, were transferred to the membrane after SDS-PAGE gel electrophoresis and probed with primary antibodies, namely FOXM1 and β-actin (Proteintech). Following a wash with TBS-T, the membranes were incubated with anti-rabbit and anti-mouse secondary antibodies, and subsequent imaging was performed.[16,20]

### 4.3.4 | Statistical analysis

Statistical analysis was performed using the Student's *t* test and *p* values less than 0.05 was considered as statistically significant and denoted by an asterisk in the figures.

## ACKNOWLEDGMENTS

Khaled A. N. Abusharkh thanks the Council of Higher Education of Türkiye (YÖK Palestine Scholarship) and Al-Quds University in Palestine for the scholarship awarded. The authors would like to thank Prof. Dr. Ahmet Ceyhan Gören from Gebze Technical University for performing 2D NMR analysis for compounds. The authors gratefully acknowledge the laboratory facilities and spectroscopic analysis provided by Çanakkale Onsekiz Mart University Experimental Research Application and Research Center (ÇOMÜDAM), Science and Technology Application and Research Center (ÇOBİLTUM), Çankırı Karatekin University Central Research Laboratory Application and Research Center, and Central Research Application Laboratory, Gebze Technical University. The funding for this research was provided by Çanakkale Onsekiz Mart University Research Coordination Unit (Project Number: FDK-2022-4145).

## CONFLICTS OF INTEREST STATEMENT

The authors declare no conflicts of interest.

## DATA AVAILABILITY STATEMENT

The data that support the findings of this study are available in the Supporting Information of this article.

## ORCID

*Ferah Comert Onder* https://orcid.org/0000-0002-4037-1979
*Merve Sıkık* http://orcid.org/0000-0003-2552-038X
*Mehmet Ay* http://orcid.org/0000-0002-1095-1614

## REFERENCES

[1] T. V. Kalin, V. Ustiyan, V. V. Kalinichenko, *Cell Cycle* **2011**, *10*, 396. https://doi.org/10.4161/cc.10.3.14709
[2] N. Zhang, P. Wei, A. Gong, W. T. Chiu, H. T. Lee, H. Colman, H. Huang, J. Xue, M. Liu, Y. Wang, R. Sawaya, K. Xie, W. K. A. Yung, R. H. Medema, X. He, S. Huang, *Cancer Cell* **2011**, *20*, 427. https://doi.org/10.1016/j.ccr.2011.08.016
[3] X. Wang, H. Kiyokawa, M. B. Dennewitz, R. H. Costa, *Proc. Natl. Acad. Sci. U. S. A.* **2002**, *99*, 16881. https://doi.org/10.1073/pnas.252570299
[4] Z. Hamurcu, N. Delibaşı, U. Nalbantoglu, E. F. Sener, N. Nurdinov, B. Tascı, S. Taheri, Y. Özkul, H. Donmez-Altuntas, H. Canatan, B. Ozpolat, *J. Mol. Med.* **2019**, *97*, 491. https://doi.org/10.1007/s00109-019-01750-8
[5] M. Halasi, A. L. Gartel, *Mol. Cancer Ther.* **2013**, *12*, 245. https://doi.org/10.1158/1535-7163.MCT-12-0712
[6] N. Xu, D. Jia, W. Chen, H. Wang, F. Liu, H. Ge, X. Zhu, Y. Song, X. Zhang, D. Zhang, D. Ge, C. Bai, *PLoS One* **2013**, *8*, e59412. https://doi.org/10.1371/journal.pone.0059412
[7] Y. Wang, X. Zhou, M. Xu, W. Weng, Q. Zhang, Y. Yang, P. Wei, X. Du, *Oncotarget*. **2016**, *7*, 36681. https://doi.org/10.18632/oncotarget.9160
[8] N. Wen, Y. Wang, L. Wen, S. H. Zhao, Z. H. Ai, Y. Wang, B. Wu, H. X. Lu, H. Yang, W. C. Liu, Y. Li, *J. Transl. Med.* **2014**, *12*, 134. https://doi.org/10.1186/1479-5876-12-134
[9] W. Guo, L. Lin, X. He, F. He, C. Wang, N. Chen, Y. Wang, *Critical Reviews™ in Oncogenesis* **2017**, *22*, 427. https://doi.org/10.1615/CritRevOncog.2017020575
[10] S. Narrandes, S. Huang, L. Murphy, W. Xu, *BMC Cancer* **2018**, *18*, 22. https://doi.org/10.1186/s12885-017-3939-4
[11] M. C. Abba, E. Lacunza, M. Butti, C. M. Aldaz, *Biomarker Insights* **2010**, *5*, BMI.S5740. https://doi.org/10.4137/BMI.S5740
[12] R. Bayraktar, C. Ivan, E. Bayraktar, P. Kanlikilicer, N. N. Kabil, N. Kahraman, H. A. Mokhlis, D. Karakas, C. Rodriguez-Aguayo, A. Arslan, J. Sheng, S. Wong, G. Lopez-Berestein, G. A. Calin, B. Ozpolat, *Clin. Cancer Res.* **2018**, *24*, 4225. https://doi.org/10.1158/1078-0432.CCR-17-1959
[13] O. Engebraaten, H. K. M. Vollan, A.-L. Børresen-Dale, *Am. J. Pathol.* **2013**, *183*, 1064. https://doi.org/10.1016/j.ajpath.2013.05.033
[14] P. Raychaudhuri, H. J. Park, *Cancer Res.* **2011**, *71*, 4329. https://doi.org/10.1158/0008-5472.CAN-11-0640

[15] C. Pilarsky, M. Wenzig, T. Specht, H. D. Saeger, R. Grützmann, *Neoplasia* **2004**, *6*, 744. https://doi.org/10.1593/neo.04277

[16] V. Cınar, Z. Hamurcu, A. Guler, N. Nurdinov, B. Ozpolat, *Breast Cancer* **2022**, *29*, 1106. https://doi.org/10.1007/s12282-022-01391-9

[17] Z. Hamurcu, N. Kahraman, A. Ashour, B. Ozpolat, *Breast Cancer Res. Treat.* **2017**, *163*, 485. https://doi.org/10.1007/s10549-017-4207-7

[18] Z. Hamurcu, A. Ashour, N. Kahraman, B. Ozpolat, *Oncotarget* **2016**, *7*, 16619. https://doi.org/10.18632/oncotarget.7672

[19] F. Comert Onder, N. Kahraman, E. Bellur Atici, A. Cagir, H. Kandemir, G. Tatar, T. Taskin Tok, G. Kara, B. Karliga, S. Durdagi, M. Ay, B. Ozpolat, *ACS Pharmacol. Transl. Sci.* **2021**, *4*, 926. https://doi.org/10.1021/acsptsci.1c00030

[20] K. A. N. Abusharkh, F. Comert Onder, V. Çınar, Z. Hamurcu, B. Ozpolat, M. Ay, *Med. Oncol.* **2024**, *41*, 188. https://doi.org/10.1007/s12032-024-02427-0

[21] X. Song, S. S. Fiati Kenston, J. Zhao, D. Yang, Y. Gu, *Med. Oncol.* **2017**, *34*, 41. https://doi.org/10.1007/s12032-017-0888-3

[22] T. V. Kalin, I.-C. Wang, T. J. Ackerson, M. L. Major, C. J. Detrisac, V. V. Kalinichenko, A. Lyubimov, R. H. Costa, *Cancer Res.* **2006**, *66*, 1712. https://doi.org/10.1158/0008-5472.CAN-05-3138

[23] M. Liu, B. Dai, S.-H. Kang, K. Ban, F.-J. Huang, F. F. Lang, K. D. Aldape, T. Xie, C. E. Pelloski, K. Xie, R. Sawaya, S. Huang, *Cancer Res.* **2006**, *66*, 3593. https://doi.org/10.1158/0008-5472.CAN-05-2912

[24] Z. Zhang, S. Xue, Y. Gao, Y. Li, Z. Zhou, J. Wang, Z. Li, Z. Liu, *Cell Death Discov.* **2022**, *8*, 280. https://doi.org/10.1038/s41420-022-01070-w

[25] I.-M. Kim, T. Ackerson, S. Ramakrishna, M. Tretiakova, I.-C. Wang, T. V. Kalin, M. L. Major, G. A. Gusarova, H. M. Yoder, R. H. Costa, V. V. Kalinichenko, *Cancer Res.* **2006**, *66*, 2153. https://doi.org/10.1158/0008-5472.CAN-05-3003

[26] Y. Yoshida, I. C. Wang, H. M. Yoder, N. O. Davidson, R. H. Costa, *Gastroenterology* **2007**, *132*, 1420. https://doi.org/10.1053/j.gastro.2007.01.036

[27] S. Uddin, M. Ahmed, A. Hussain, J. Abubaker, N. Al-Sanea, A. AbdulJabbar, L. H. Ashari, S. Alhomoud, F. Al-Dayel, Z. Jehan, P. Bavi, A. K. Siraj, K. S. Al-Kuraya, *Am. J. Pathol.* **2011**, *178*, 537. https://doi.org/10.1016/j.ajpath.2010.10.020

[28] O. A. Kalinina, S. A. Kalinin, E. W. Polack, I. Mikaelian, S. Panda, R. H. Costa, G. R. Adami, *Oncogene* **2003**, *22*, 6266. https://doi.org/10.1038/sj.onc.1206640

[29] H. Okabe, S. Satoh, T. Kato, O. Kitahara, R. Yanagawa, Y. Yamaoka, T. Tsunoda, Y. Furukawa, Y. Nakamura, *Cancer Res.* **2001**, *61*, 2129. https://pubmed.ncbi.nlm.nih.gov/11280777/

[30] J. Akhtar, A. A. Khan, Z. Ali, R. Haider, M. Shahar Yar, *Eur. J. Med. Chem.* **2017**, *125*, 143. https://doi.org/10.1016/j.ejmech.2016.09.023

[31] R. S. Keri, M. R. Patil, S. A. Patil, S. Budagumpi, *Eur. J. Med. Chem.* **2015**, *89*, 207. https://doi.org/10.1016/j.ejmech.2014.10.059

[32] P. Venkatesh, P. Venkatesh, S. N. Pandeya, *Int. J. ChemTech Res.* **2009**, *1*, 1354. https://sphinxsai.com/ctvol4/ct_pdf_vol_4/ct=92%20(1354–1358).pdf

[33] E. Meltzer-Mats, G. Babai-Shani, L. Pasternak, N. Uritsky, T. Getter, O. Viskind, J. Eckel, E. Cerasi, H. Senderowitz, S. Sasson, A. Gruzman, *J. Med. Chem.* **2013**, *56*, 5335. https://doi.org/10.1021/jm4001488

[34] V. S. Padalkar, V. D. Gupta, K. R. Phatangare, V. S. Patil, P. G. Umape, N. Sekar, *J. Saudi Chem. Soc.* **2014**, *18*, 262. https://doi.org/10.1016/j.jscs.2011.07.001

[35] J. Cai, M. Sun, X. Wu, J. Chen, P. Wang, X. Zong, M. Ji, *Eur. J. Med. Chem.* **2013**, *63*, 702. https://doi.org/10.1016/j.ejmech.2013.03.013

[36] X. H. Shi, Z. Wang, Y. Xia, T. H. Ye, M. Deng, Y. Z. Xu, Y. Q. Wei, L. T. Yu, *Molecules* **2012**, *17*, 3933. https://doi.org/10.3390/molecules17043933

[37] C. O. Leong, M. Suggitt, D. J. Swaine, M. C. Bibby, M. F. G. Stevens, T. D. Bradshaw, *Mol. Cancer Ther.* **2004**, *3*, 1565. https://doi.org/10.1158/1535-7163.1565.3.12

[38] F. Eshkil, H. Eshghi, A. S. Saljooghi, M. Bakavoli, M. Rahimizadeh, *Russ. J. Bioorg. Chem.* **2017**, *43*, 576. https://doi.org/10.1134/S1068162017050065

[39] A. Irfan, F. Batool, S. A. Zahra Naqvi, A. Islam, S. M. Osman, A. Nocentini, S. A. Alissa, C. T. Supuran, *J. Enzyme Inhib. Med. Chem.* **2020**, *35*, 265. https://doi.org/10.1080/14756366.2019.1698036

[40] K. S. Shukla, S. Pandey, P. Chawla, *Antiinfect Agents* **2018**, *17*, 115. https://doi.org/10.2174/2211352516666181024151213

[41] P. Saralkar, W. J. Geldenhuys, *Med. Chem. Res.* **2019**, *28*, 2165. https://doi.org/10.1007/s00044-019-02444-z

[42] M. J. Naim, M. J. Alam, S. Ahmad, F. Nawaz, N. Shrivastava, M. Sahu, O. Alam, *Eur. J. Med. Chem.* **2017**, *129*, 218. https://doi.org/10.1016/j.ejmech.2017.02.031

[43] Z. M. M. Alzhrani, M. M. Alam, T. Neamatallah, S. Nazreen, *J. Enzyme Inhib. Med. Chem.* **2020**, *35*, 1116. https://doi.org/10.1080/14756366.2020.1759581

[44] A. H. Abdelazeem, A. M. Gouda, H. A. Omar, M. F. Tolba, *Bioorg. Chem.* **2014**, *57*, 132. https://doi.org/10.1016/j.bioorg.2014.10.001

[45] A. Bordessa, C. Colin-Cassin, I. Grillier-Vuissoz, S. Kuntz, S. Mazerbourg, G. Husson, M. Vo, S. Flament, H. Martin, Y. Chapleur, M. Boisbrun, *Eur. J. Med. Chem.* **2014**, *83*, 129. https://doi.org/10.1016/j.ejmech.2014.06.015

[46] M. Azizmohammadi, M. Khoobi, A. Ramazani, S. Emami, A. Zarrin, O. Firuzi, R. Miri, A. Shafiee, *Eur. J. Med. Chem.* **2013**, *59*, 15. https://doi.org/10.1016/j.ejmech.2012.10.044

[47] K. Tilekar, N. Upadhyay, M. Schweipert, J. D. Hess, L. H. Macias, P. Mrowka, F. J. Meyer-Almes, R. J. Aguilera, C. V. Iancu, J. Choe, C. S. Ramaa, *Eur. J. Pharm. Sci.* **2020**, *154*, 105512. https://doi.org/10.1016/j.ejps.2020.105512

[48] T. Durai Ananda Kumar, N. Swathi, J. Navatha, C. V. S. Subrahmanyam, K. Satyanarayana, *J. Sulfur Chem.* **2015**, *36*, 105. https://doi.org/10.1080/17415993.2014.970555

[49] Q. Xiang, G. Tan, X. Jiang, K. Wu, W. Tan, Y. Tan, *Sci. Rep.* **2017**, *7*, 45377. https://doi.org/10.1038/srep45377

[50] O. Afzal, M. S. Akhtar, S. Kumar, M. R. Ali, M. Jaggi, S. Bawa, *Eur. J. Med. Chem.* **2016**, *121*, 318. https://doi.org/10.1016/j.ejmech.2016.05.038

[51] S. Prasanna, R. J. Doerksen, *Curr. Med. Chem.* **2009**, *16*, 21. https://doi.org/10.2174/092986709787002817

[52] N. Bhogireddy, G. Kumar Veeramachaneni, N. Vamsi, K. Ambatipudi, P. Mathi, J. Ippaguntla, U. R. Ganta, S. G. Adusumalli, V. R. Bokka, *Bioinformation* **2013**, *9*, 788. https://doi.org/10.6026/97320630009788

[53] S. Jelfs, P. Ertl, P. Selzer, *J. Chem. Inf. Model.* **2007**, *47*, 450. https://doi.org/10.1021/ci600285n

[54] D. R. Littler, M. Alvarez-Fernandez, A. Stein, R. G. Hibbert, T. Heidebrecht, P. Aloy, R. H. Medema, A. Perrakis, *Nucleic Acids Res.* **2010**, *38*, 4527. https://doi.org/10.1093/nar/gkq194

[55] F. Fontaine, J. Overman, M. François, *Cell Regen.* **2015**, *4*, 4:2. https://doi.org/10.1186/s13619-015-0015-x

[56] G. Luo, X. Lin, A. Vega-Medina, M. Xiao, G. Li, H. Wei, C. A. Velázquez-Martínez, H. Xiang, *J. Med. Chem.* **2021**, *64*, 17098. https://doi.org/10.1021/acs.jmedchem.1c01069

[57] S. A. Tabatabaei-Dakhili, R. Aguayo-Ortiz, L. Domínguez, C. A. Velázquez-Martínez, *J. Mol. Graph. Model.* **2018**, *80*, 197. https://doi.org/10.1016/j.jmgm.2018.01.009

[58] S. A. Tabatabaei Dakhili, D. J. Pérez, K. Gopal, S. Y. Tabatabaei Dakhili, J. R. Ussher, C. A. Velázquez-Martínez, *Bioorg. Chem.* **2019**, *93*, 103269. https://doi.org/10.1016/j.bioorg.2019.103269

[59] S. A. Tabatabaei Dakhili, D. J. Pérez, K. Gopal, M. Haque, J. R. Ussher, K. Kashfi, C. A. Velázquez-Martínez, *Eur. J. Med. Chem.* **2021**, *209*, 112902. https://doi.org/10.1016/j.ejmech.2020.112902

[60] S. K. Radhakrishnan, U. G. Bhat, D. E. Hughes, I. C. Wang, R. H. Costa, A. L. Gartel, *Cancer Res.* **2006**, *66*, 9731. https://doi.org/10.1158/0008-5472.CAN-06-1576

[61] M. Halasi, A. L. Gartel, *Cell Cycle* **2009**, *8*, 1966. https://doi.org/10.4161/cc.8.12.8708

[62] S. Shukla, D. Milewski, A. Pradhan, N. Rama, K. Rice, T. Le, M. J. Flick, S. Vaz, X. Zhao, K. D. Setchell, E. Logarinho, V. V. Kalinichenko, T. V. Kalin, *Mol. Cancer Ther.* **2019**, *18*, 1217. https://doi.org/10.1158/1535-7163.MCT-18-0709

[63] M. S. Chesnokov, M. Halasi, S. Borhani, Z. Arbieva, B. N. Shah, R. Oerlemans, I. Khan, C. J. Camacho, A. L. Gartel, *Cell Death Dis.* **2021**, *12*, 704. https://doi.org/10.1038/s41419-021-03978-0

[64] M. Halasi, B. Hitchinson, B. N. Shah, R. Váraljai, I. Khan, E. V. Benevolenskaya, V. Gaponenko, J. L. Arbiser, A. L. Gartel, *Cell Death Dis.* **2018**, *9*, 84. https://doi.org/10.1038/s41419-017-0156-7

[65] K. Ulhaka, K. Kanokwiroon, M. Khongkow, R. Bissanum, T. Khunpitak, P. Khongkow, *Int. J. Mol. Sci.* **2021**, *22*, 6685. https://doi.org/10.3390/ijms22136685

[66] M. V. Gormally, T. S. Dexheimer, G. Marsico, D. A. Sanders, C. Lowe, D. Matak-Vinković, S. Michael, A. Jadhav, G. Rai, D. J. Maloney, A. Simeonov, S. Balasubramanian, *Nat. Commun.* **2014**, *5*, 5165. https://doi.org/10.1038/ncomms6165

[67] S. Raghuwanshi, X. Zhang, Z. Arbieva, I. Khan, H. Mohammed, Z. Wang, A. Domling, C. J. Camacho, A. L. Gartel, *Cell Death Discov.* **2024**, *10*, 211. https://doi.org/10.1038/s41420-024-01929-0

[68] U. G. Bhat, M. Halasi, A. L. Gartel, *PLoS One* **2009**, *4*, e6593. https://doi.org/10.1371/journal.pone.0006593

[69] A. L. Gartel, *Cell Cycle* **2011**, *10*, 4341. https://doi.org/10.4161/cc.10.24.18544

[70] V. Petrovic, R. H. Costa, L. F. Lau, P. Raychaudhuri, A. Tyner, *Cancer Biol. Ther.* **2010**, *9*, 1008. https://doi.org/10.4161/cbt.9.12.11710

[71] I. A. Y. Ghannam, E. A. Abd El-Meguid, I. H. Ali, D. H. Sheir, A. M. El Kerdawy, *Bioorg. Chem.* **2019**, *93*, 103373. https://doi.org/10.1016/j.bioorg.2019.103373

[72] H. Xie, D. Ng, S. N. Savinov, B. Dey, P. D. Kwong, R. Wyatt, A. B. Smith, W. A. Hendrickson, *J. Med. Chem.* **2007**, *50*, 4898. https://doi.org/10.1021/jm070564e

[73] M. Majdecki, P. Niedbala, J. Jurczak, *Org. Lett.* **2019**, *21*, 8085. https://doi.org/10.1021/acs.orglett.9b03065

[74] M. S. Alves Palma, *MOJ Bioorg. Org. Chem.* **2017**, *1*, 122. https://doi.org/10.15406/mojboc.2017.01.00022

[75] B. S. Londhe, U. R. Pratap, J. R. Mali, R. A. Mane, *Bull. Korean Chem. Soc.* **2010**, *31*, 2329. https://doi.org/10.5012/bkcs.2010.31.8.2329

[76] G. Bruno, L. Costantino, C. Curinga, R. Maccari, F. Monforte, F. Nicolò, R. Ottanà, M. G. Vigorita, *Bioorg. Med. Chem.* **2002**, *10*, 1077. https://doi.org/10.1016/S0968-0896(01)00366-2

[77] I. M. Da Silva, J. Da Silva Filho, P. B. G. S. Santiago, M. S. do Egito, C. A. de Souza, F. L. Gouveia, R. M. Ximenes, K. de Sena, A. R. de Faria, D. J. Brondani, J. de Albuquerque, *BioMed Res. Int.* **2014**, *2014*, 1. https://doi.org/10.1155/2014/316082

[78] E. Cortelazzo-Polisini, M. Boisbrun, A. H. Gansmüller, C. Comoy, *J. Org. Chem.* **2022**, *87*, 9699. https://doi.org/10.1021/acs.joc.2c00748

[79] P. T. Tryambake, *Asian J. Chem.* **2017**, *29*, 2401. https://doi.org/10.14233/ajchem.2017.20695

[80] K. Tilekar, N. Upadhyay, J. D. Hess, L. H. Macias, P. Mrowka, R. J. Aguilera, F. J. Meyer-Almes, C. V. Iancu, J. Choe, C. S. Ramaa, *Eur. J. Med. Chem.* **2020**, *202*, 112603. https://doi.org/10.1016/j.ejmech.2020.112603

[81] H. El-Kashef, G. Badr, N. Abo El-Maali, D. Sayed, P. Melnyk, N. Lebegue, R. Abd El-Khalek, *Bioorg. Chem.* **2020**, *96*, 103569. https://doi.org/10.1016/j.bioorg.2020.103569

[82] F. S. M. Neri, D. B. C. Júnior, T. Q. Froes, P. B. G. da Silva, M. S. do Egito, P. O. L. Moreira, F. de Pilla Varotti, M. S. Castilho, R. G. Teixeira-Neto, J. F. C. de Albuquerque, F. H. A. Leite, *Parasitol. Res.* **2020**, *119*, 2263. https://doi.org/10.1007/s00436-020-06706-3

[83] S. D. Fazylov, O. A. Nurkenov, S. K. Amerkhanova, I. S. Tolepbek, *Russ. J. Gen. Chem.* **2013**, *83*, 1792. https://doi.org/10.1134/S1070363213090284

[84] C. A. Lipinski, F. Lombardo, B. W. Dominy, P. J. Feeney, *Adv. Drug Deliv. Rev.* **2001**, *46*, 3. https://doi.org/10.1016/s0169-409x(00)00129-0

[85] N. M. O'Boyle, M. Banck, C. A. James, C. Morley, T. Vandermeersch, G. R. Hutchison, *J. Cheminf.* **2011**, *3*, 33. https://doi.org/10.1186/1758-2946-3-33

[86] G. M. Morris, R. Huey, W. Lindstrom, M. F. Sanner, R. K. Belew, D. S. Goodsell, A. J. Olson, *J. Comput. Chem.* **2009**, *30*, 2785. https://doi.org/10.1002/jcc.21256

[87] O. Trott, A. J. Olson, *J. Comput. Chem.* **2009**, *31*, 455. https://doi.org/10.1002/jcc.21334

[88] S. Kalin, F. Comert Onder, *J. Biomol. Struct. Dyn.* **2023**, *12*, 1. https://doi.org/10.1080/07391102.2023.2291830

[89] F. Comert Onder, N. Sahin, G. Davutlar, A. Onder, M. Ay, *ChemistrySelect* **2023**, *8*, e202304614. https://doi.org/10.1002/slct.202304614

[90] W. L. Jorgensen, J. Tirado-Rives, *J. Am. Chem. Soc.* **1988**, *110*, 1657. https://doi.org/10.1021/ja00214a001

[91] Onder F. C., Durdagi S., Kahraman N., Uslu T. N., Kandemir H., Atici E. B., Ozpolat B., Ay M. *Bioorg. Chem.* **2021**;*116*:105296. https://doi.org/10.1016/j.bioorg.2021.105296.

## SUPPORTING INFORMATION

Additional supporting information can be found online in the Supporting Information section at the end of this article.

**How to cite this article:** K. A. N. Abusharkh, F. Comert Onder, V. Çınar, A. Onder, M. Sıkık, Z. Hamurcu, B. Ozpolat, M. Ay, *Arch. Pharm.* **2024**;*357*:e2400504. https://doi.org/10.1002/ardp.202400504